Influence of In-induced resonant level on the normal-state and superconducting properties of Sn1.03Te

Shantanu Misra, Bartlomiej Wiendlocha, Janusz Tobola, Petr Levinský, Jiří Hejtmánek, Sylvie Migot, Jaafar Ghanbaja, Anne Dauscher, Bertrand Lenoir, Christophe Candolfi

Influence of In-induced resonant level on the normal-state and superconducting properties of $Sn_{1.03}Te$

Shantanu Misra[1], Bartlomiej Wiendlocha[2,*], Janusz Tobola[2], Petr Levinský[3], Jiří Hejtmánek[3], Sylvie Migot[1], Jaafar Ghanbaja[1], Anne Daucher[1], Bertrand Lenoir[1], Christophe Candolfi[1,*]

[1] *Institut Jean Lamour, UMR 7198 CNRS – Université de Lorraine, 2 allée André Guinier-Campus ARTEM, BP 50840, 54011 Nancy Cedex, France*

[2] *Faculty of Physics and Applied Computer Science, AGH University of Science and Technology, Aleja Mickiewicza 30, 30-059 Krakow, Poland*

[3] *Institute of Physics, Czech Academy of Sciences, Cukrovarnická 10, 162 00, Praha 6, Czech Republic*

* Corresponding authors:

wiendlocha@fis.agh.edu.pl (BW);

christophe.candolfi@mines-nancy.univ-lorraine.fr (CC)

Abstract

Normal-state transport properties (2 – 300 K) of the polycrystalline series $Sn_{1.03-\delta-x}In_xTe$ ($0 \leq x \leq 0.07$; $\delta \leq 0.0025$) were investigated by means of electrical resistivity, thermopower, Hall effect and thermal conductivity measurements. The distortion of the valence band structure by the In-induced resonant level (RL) has a profound influence on the evolution of the normal-state

properties with x and on the emergence of superconductivity evidenced by specific heat measurements down to 0.35 K. In addition to a nearly forty-fold increase in the residual electrical resistivity ρ_0 on going from x = 0.0 to 0.05, the thermopower α shows a nonlinear, complex behavior as a function of both temperature and x. While Hall measurements indicate a dominant holelike response across the entire composition and temperature ranges, α changes sign below about 100 K and remains negative down to 5 K for $0.0015 \leq x \leq 0.0045$. Additional measurements under magnetic fields $\mu_0 H$ of up to 14T further shows that $\alpha(\mu_0 H)$ gradually shifts towards positive values, suggestive of a dominant holelike contribution to α. Superconductivity emerges for x = 0.02 at a critical temperature $T_c = 0.67$ K, with T_c increasing with x to reach 1.73 K for x = 0.07. The variations in the superconducting parameters with x, notably the specific heat jump at T_c, confirms the results reported in prior studies and suggests a non-trivial role of the RL on the electron-phonon coupling strength. The striking similarities between this series and the canonical resonant system $Pb_{1-x}Tl_xTe$ provide an excellent experimental opportunity to gain a deeper understanding of the close interplay between resonant level, anomalous transport properties and superconductivity.

I. Introduction

Narrow-band-gap chalcogenide semiconductors continue to be of prime interest for the design of highly-efficient thermoelectric materials for applications in power generation.[1,2] The electronic band structure of most of these semiconductors can be manipulated by specific dopants that induce a distortion near the valence or conduction band edge, a mechanism known as resonant level (RL).[3-5] A significant increase in the thermopower α is observed when the chemical potential

resides in this local distortion, ultimately leading to enhanced thermoelectric properties. A canonical example of such a behavior is the *p*-type Tl-doped PbTe compounds for which the Tl atoms act as the resonant impurities.[3] In addition to this system, resonant levels have been induced in a restricted set of narrow-band-gap chalcogenide semiconductors that include Sn-doped Bi_2Te_3 and β-As_2Te_3 and In-doped GeTe.[3,6-10]

In $Pb_{1-x}Tl_xTe$, a concomitant effect to the formation of the RL is the emergence of superconductivity beyond a critical Tl concentration of around 0.3%.[11,12] What makes this observation particularly intriguing is the high critical temperatures T_c of up to 1.5 K achieved at relatively low hole densities of around 10^{20} cm^{-3}, which are unexpected based on the standard version of the BCS theory. In addition, these T_c are orders of magnitude higher than those measured in other superconducting, doped semiconductors. The difficulty to explain superconductivity in $Pb_{1-x}Tl_xTe$ with a conventional phonon-mediated pairing triggered the development of alternative scenarios. While the presence of additional carrier pockets in the Brillouin zone resulting in an increased density of states and promoting interband scattering or the creation of Te vacancies counterbalancing the additional holes provided by Tl have been proposed,[12,13] a number of circumstantial evidence points to a possible role played by charge fluctuations of the Tl atoms between Tl^+ and Tl^{3+} valence states.[14-17] This valence-skipping mechanism has been proposed theoretically to provide a superconducting pairing interaction and to give rise to a charge-Kondo effect, explaining several normal-state and superconducting properties of the $Pb_{1-x}Tl_xTe$ compounds.[18,19] Recent photoemission spectroscopy measurements have lent experimental credit to this scenario by evidencing the presence of the two valences Tl^{1+} and Tl^{3+} and the absence of a second band at the Fermi energy.[20,21]

The binary $Sn_{1-\delta}Te$ (δ is the concentration of Sn vacancies), crystallizing in a rock-salt cubic structure, exhibits an electronic band structure similar to PbTe leading to high thermoelectric performance when appropriately doped.[22-46] The presence of inherent Sn vacancies acting as double acceptors, the contribution of two valence-band maxima to the transport in highly-doped samples and a ferroelectric transition accompanied by a cubic-to-rhombohedral lattice distortion near 100 K are the main traits that distinguish SnTe from PbTe. Despite these important differences, the partial substitution of In for Sn also leads to the formation of a resonant level, which strongly influences the transport properties above room temperature.[23,26,36,45,46] While $Sn_{1-\delta}Te$ is superconducting below 0.3 K in agreement with BCS predictions, superconductivity in $Sn_{1-\delta-x}In_xTe$ strongly resembles that in $Pb_{1-x}Tl_xTe$ at low In concentrations. Doping with In significantly enhances T_c up to 2 K for an In content of around 10% with possible signs of topological superconductivity connected to the topological crystalline insulating nature of $Sn_{1-\delta}Te$.[47-52] Further increasing the In concentration to its solubility limit of 40% results in a continuous increase in T_c that ultimately reaches 4.5 K.[53-55] Due to the valence-skipping nature of In observed in various compounds,[15,56] these striking similarities with $Pb_{1-x}Tl_xTe$ suggest that a valence-fluctuation scenario may equally apply to $Sn_{1-\delta-x}In_xTe$. While prior studies have mainly focused on the evolution of superconductivity with x at high In contents,[47-55] no detailed investigation of the low-temperature transport properties and the concomitant emergence of superconductivity at low In concentrations has been reported so far. Because the non-monotonic evolution of the low-temperature thermopower in $Pb_{1-x}Tl_xTe$ has been interpreted in terms of the charge-Kondo effect,[17] it is of interest to extend these measurements to the series $Sn_{1-\delta-x}In_xTe$ and determine the extent to which both systems behave similarly. Furthermore, it is worth underlining that, so far, no theoretical studies were able to simultaneously explain the resonant enhancement of thermopower

and the presence of superconductivity, with both phenomena coexisting in the same samples in the $Pb_{1-x}Tl_xTe$ and $Sn_{1-\delta-x}In_xTe$ systems. While electronic band structure and transport calculations successfully explained thermopower enhancement in the former,[13] mixed-valence behavior, proposed to be responsible for superconductivity, is beyond density functional theory (DFT) calculations. On the other hand, the experimentally observed resonant increase in the room-temperature thermopower was not addressed by the mixed-valence and charge Kondo models. The lack of unifying physical picture of superconductivity and thermopower enhancement in $Pb_{1-x}Tl_xTe$ and $Sn_{1-\delta-x}In_xTe$ motivate further theoretical and experimental studies.

Here, we provide a comprehensive study of the transport and galvanomagnetic properties of the self-compensated In-doped $Sn_{1.03-\delta-x}In_xTe$ series for x varying between 0.0 and 0.07 between 2 and 300 K. These results are complemented by thermodynamic measurements performed down to 0.35 K. The introduction of Sn excess in the nominal composition was used as an efficient mean to decrease the concentration of Sn vacancies δ to its minimum value (~0.0025) that tunes the position of the chemical potential in the In-induced RL. We show that the resonant nature of In gives rise to signatures on normal-state transport properties similar to those observed in Tl-doped PbTe.[17] In particular, the thermopower α experiences sign changes upon cooling below 100 K, which strongly depends on x despite the very low In concentrations probed. Our results confirm the development of a superconducting state above 0.35 K for $x \geq 0.02$, with several x-dependent anomalies that points to a central role played by the RL in enhancing the critical temperature T_c. The distinct role of In in $Sn_{1-\delta}Te$ is supported by DFT calculations of the residual electrical resistivity and carrier lifetime inferred from the shape of the Bloch spectral functions (BSF).

II. Experimental and computational details

Polycrystalline samples of $Sn_{1.03-\delta-x}In_xTe$ with nominal compositions x = 0.0, 0.0005, 0.0015, 0.0025, 0.0035, 0.0045, 0.0100 and 0.0200 were synthesized by powder metallurgy. Transport properties measurements indicated that the concentration of Sn vacancies are likely decreasing with increasing x, possibly disappearing above x = 0.02. For this reason, the additional x = 0.05 and 0.07 samples were prepared without Sn excess (that is, starting from the nominal compositions $Sn_{1-x}In_xTe$). Prior to use, elemental Sn, In and Te (5N, 99.999%) were purified to remove any traces of oxides. These materials were sealed under high vacuum in a quartz glass tube and kept in a rocking furnace for 5h at 1100 K. The tubes were then quenched in room-temperature water. The obtained ingots were hand-ground into fine powders inside an argon-filled glove box. The powders were consolidated by Spark Plasma Sintering at 750 K in a graphite die for 10 min under an uniaxial pressure of 65 MPa. All the samples show a relative density of more than 96% of the theoretical density. The dense cylindrical pellets were then cut into rectangular bar-shaped samples of typical dimensions $8\times2\times2$ mm^3 for transport property measurement.

The crystal structure and phase purity were verified by powder X-ray diffraction (PXRD) at 300 K using a D8 Advance diffractometer (Bruker). Chemical composition and homogeneity was assessed by electron dispersive X-ray spectroscopy (EDXS) using a Quanta FEG scanning electron microscope. Transmission and scanning electron microscopy (TEM – STEM) analyses were performed on a thin slice of the x = 0.02 sample prepared by the dual focused ion beam (FIB) – scanning electron microscope system using the in situ lift-out technique. STEM images in high-angle annular dark-field (HAADF) mode were collected with a JEOL ARM 200F – cold FEG TEM/STEM microscope equipped with a spherical aberration (CS) probe and image correctors

and operating at 200 keV. EDXS analyses were further realized to assess the chemical homogeneity at the nm scale.

Low-temperature electrical resistivity, thermopower and thermal conductivity (5 – 300 K) were simultaneously measured in the continuous mode using the thermal transport option of a physical property measurement system (PPMS, Quantum Design). Additional measurements under magnetic fields $\mu_0 H$ of up to 14T were performed between 5 and 120 K. Hall effect measurements were performed using the ac transport option of the PPMS between 5 and 300 K. The Hall resistivity ρ_H was determined by measurements of the transverse electrical resistivity ρ_{xy} under magnetic field reversal following the relation $\rho_H = \left[\rho_{xy}(+\mu_0 H) - \rho_{xy}(-\mu_0 H)\right]/2$. The Hall coefficient R_H was derived from the slope of the $\rho_H(\mu_0 H)$ data for fields $-1 \leq \mu_0 H \leq 1$T. The Hall carrier concentration p_H and the Hall mobility μ_H were determined from the single-band relations $p_H = 1/R_H e$ and $\mu_H = R_H/\rho$ where e is the electron charge. We note that the second, heavy-hole valence band starts to contribute to the transport at high temperatures for pristine and lightly-doped $Sn_{1-\delta}Te$ samples,[22-26,44] making the use of single-band formulas reasonable below 300 K. Specific heat measurements were performed in the temperature ranges 1.8 – 10 and 0.4 – 4 K using the ^{4}He and ^{3}He option, respectively, of the PPMS. Both measurements were performed on the same small polycrystalline piece (approximately 15 mg) glued onto the sample holder by a minute amount of Apiezon N grease.

Electronic band structure calculations were done using the Korringa-Kohn-Rostoker (KKR) method with the coherent potential approximation (CPA), applied to simulate the presence of dopant atoms. The Munich SPRKKR package was used.[58,59] The experimentally-determined rock-salt crystal structure and lattice parameter (6.32 Å) were used. Regular *k*-point mesh was considered in calculations, with the irreducible part of the Brillouin zone (BZ) sampled with 2500

k-points for the self-consistent cycle and 2×10^5 for the density of states (DOS) and Bloch spectral density functions (BSF) calculations. The local density approximation (LDA) version of Vosko, Wilk and Nussair was used to construct the effective crystal potential.[60] For all atoms, angular momentum cut-off $l_{max} = 3$ was set and full-potential full-relativistic calculations were performed. High convergence limits were put on the self-consistent cycle (10^{-5} Ry for the Fermi level E_F and for the total energy). The position of E_F was obtained using the Lloyd formula.[58,61] In addition, the zero-temperature electrical conductivity was calculated using the Kubo-Greenwood formalism,[58,62-64] with the spherical potential approximation.

III. Results

A. Electronic band structure calculations

Figure 1 presents the calculated electronic band structure and densities of states near the band gap of SnTe. The calculated value of the band gap is about 0.16 eV, which is very close to the experimental one (0.18 eV at 300 K).[27] Panel (a) shows the case of SnTe containing a small amount of Sn vacancies (0.32%, corresponding to a hole carrier concentration of 10^{20} cm^{-3} typically measured in real samples), while panels (b-d) show the effect of In with increasing In concentration from 2% to 7%. As discussed in previous studies (Refs. 45 and 46), we observe the formation of the resonant state on 5*s* orbitals of In, which is evidenced by a "hump" in DOS curve near the valence band edge, well seen in panel (b), in contrast to the rigid-band-like behavior induced by Sn vacancies in panel (a). As characteristic for the presence of a resonant impurity,[13,46] we observe an accompanying strong smearing of the resonantly-distorted valence band. Such a

band-smearing effect was experimentally observed by ARPES measurements on single-crystalline In-doped SnTe for x = 4.5%.[65] When the concentration of In increases (Figures 1c and 1d), both the DOS hump and the region of the band smearing broadens, reaching the width of the L-Σ band, which determines the normal-state transport properties of the studied material. As discussed below, this qualitatively explains the "saturation" tendency of the resonant level, that is, the electronic transport properties of the system do not change significantly above 2% of In doping.

Figure 2 presents the Bloch spectral functions plotted for a single k-vector as a function of energy. We have chosen a *k*-point k_s marked in Fig. 1, which is located halfway between the L and Σ points as a representative one. However, this specific choice has no consequences on the qualitative conclusions we draw here. For a non-resonant impurity (Sn vacancy), shown in panel (a), this single-point BSF adopts the shape of the Lorenz function (see Refs. 13, 64 and 66) and its full width at half maximum Δ corresponds to the carrier lifetime $\tau = \hbar/\Delta$ of about 2.6×10^{-13} s ($\hbar$ is the reduced Planck constant). For the resonant In dopant (Figures 2b to 2d), the BSF can no longer be described by a single Lorentzian. A rough estimate of τ indicates a drop by two orders of magnitude to 10^{-15} s, for the heavy In doped case. This effect was in details analyzed in previous studies (Ref. 13 and 67) and allows to detect the presence of the resonant state through measurements of the low-temperature residual electrical resistivity and carrier mobility. The important observation made here is that the BSF width saturates for higher In concentrations, and the effect of resonance band smearing does not increase further above 5%. As shown below, the experimental data confirms this predicted trend as a function of the In concentration.

B. Crystal structure and phase purity

The x-ray diffraction patterns of powdered samples of $Sn_{1.03-\delta-x}In_xTe$ evidenced that all samples crystallize with a cubic lattice described in the $Fm\bar{3}m$ space group (Figure 3). The Sn excess intentionally introduced to pin the Sn vacancy concentration to its lowest value ($\delta \sim 0.0025$) is the only secondary phase visible on the PXRD patterns. In agreement with prior studies, *a* tends to plateau below $x = 0.01$ ($a = 6.3242(2)$ Å for $x = 0.0$) before monotonically decreasing with increasing x up to $x = 0.07$ ($a = 6.3197(2)$ Å for $x = 0.02$ and $6.3140(2)$ Å for $x = 0.07$). SEM analyses did not evidence the presence of secondary phases other than elemental Sn at the µm scale. For $x \leq 0.01$, SEM images did not evidence the presence of In-rich areas suggesting a homogeneous spatial distribution of In. We note that the substitution levels probed are too low to make the x-ray mapping of In meaningful. For this reason, the nominal x value will be used hereafter as an adequate representation of the actual In concentration. The elemental x-ray maps collected on the $x = 0.02$, 0.05 and 0.07 samples show an overall good chemical homogeneity, with notably a homogeneous spatial distribution of In. The chemical homogeneity of the $x = 0.02$ sample was further investigated by scanning transmission electron microscopy (Figure 4). The EDXS mappings evidence the homogeneous spatial distribution of In without any evident signs of In-rich phases or segregation of In down to this scale. In agreement with prior results on the binary $Sn_{1-\delta}Te$,[44] elemental Sn is observed at the grain boundaries due to the Sn excess used in samples with In concentrations lower than $x = 0.02$.

B. Normal-state transport properties

The temperature dependences of the electrical resistivity ρ for the series $Sn_{1.03-\delta-x}In_xTe$ are presented in Figure 5a. For all samples, ρ exhibits metallic character, consistent with the degenerate nature of transport in $Sn_{1-\delta}Te$.[44,68-70] Despite the low In doping levels studied, ρ significantly increases with increasing x from 1.4 μΩ.m for x = 0.0 up to 9.5 μΩ.m for x = 0.05 at 300 K. The monotonic evolution with x in this concentration range no longer holds upon increasing x to 0.07. The large difference in ρ ($\rho(x = 0.05)\ /\rho(x = 0.0) \approx 5.6$ at 300 K) is enhanced upon cooling resulting in a strong increase in the residual electrical resistivity ρ_0 on going from x = 0.0 to x = 0.05 ($\rho(x = 0.05)\ /\rho(x = 0.0) \approx 430$ at 5 K). For all samples, the slight but noticeable change in the slope observed below about 100 K corresponds to the well-documented ferroelectric structural phase transition.[71-74] (Figure 5b). Prior studies showed that the structural phase transition temperature T_{SPT} tends to decrease with increasing the hole concentration p_H from 100 K at ~ 10^{20} cm^{-3} to 0 K at ~ 10^{21} cm^{-3}. In the present series, T_{SPT} was estimated using the midpoint of the change in the first derivative $\partial\rho/\partial T$. The lower hole concentration achieved in the x = 0.0 sample due to the Sn excess explains the increase in T_{SPT} to 112 K. In agreement with the expected trend in $T_{\mathrm{SPT}}(p_H)$, T_{SPT} smoothly decreases with increasing the In content to 76 K in the x = 0.02 sample and is no longer discernible in the x = 0.05 and 0.07 samples.

The fact that $T_{\mathrm{SPT}}(p_H)$ follows the trend observed in self-doped $Sn_{1-\delta}Te$ suggests that In behaves as an acceptor. The magnetic field variations of the transverse electrical resistivity $\rho_{xy}(\mu_0 H)$ and the inferred temperature dependence of p_H, shown in Figures 6a and 6b, respectively, confirm this behavior. Across the entire temperature and In concentration ranges, ρ_H varies linearly with $\mu_0 H$ within the magnetic field range covered, indicating that a single hole type

dominates the transport. p_H hardly evolves upon cooling, in agreement with the degenerate nature of the transport, and increases continuously with increasing the In content at 300 K from 8.0×10^{19} cm^{-3} for x = 0.0 to 1.2×10^{21} cm^{-3} for x = 0.07. This increase in p_H is accompanied by a strong decrease in the Hall mobility μ_H values at 5 K, which drop by three orders of magnitude from 3200 $cm^2\ V^{-1}\ s^{-1}$ for x = 0.0 to 9 $cm^2\ V^{-1}\ s^{-1}$ for x = 0.07 (Figure 6c). Furthermore, a progressive change in the scattering mechanisms occurs concomitantly with increasing x. While $\mu_H(T)$ follows a $T^{-0.5}$ law in the x = 0.0 sample above 30 K characteristic of alloy scattering,[44] $\mu_H(T)$ remains nearly constant ($\propto T^0$) over the entire temperature range for $x \geq 0.02$. This dependence is consistent with the strong valence band smearing induced by the presence of In resonant state (see Figure 1). At higher In concentrations and below room temperature, electron-phonon scattering is weaker than the temperature-independent resonant scattering, giving rise to the observed weak temperature dependence of the charge carrier mobility. Phonon-induced scattering of charge carriers becomes more important above room temperature, with a continuous increase in electrical resistivity being observed experimentally.[46]

Measurements of the temperature dependence of the thermopower α, shown in Figure 7a, reveal a complex evolution with both temperature and x. At 300 K, α increases with increasing x up to x = 0.02, before slightly decreasing with further increasing x to 0.07. No simple trend between α and x emerges at lower temperatures. The strongly non-linear $\alpha(T)$ of $Sn_{1.03}Te$ has been attributed to the presence of a positive phonon-drag contribution superimposed to the diffusion thermopower expected to vary linearly with temperature for a degenerate hole gas.[44] An In concentration as low as 0.05% is sufficient to significantly lower the phonon drag contribution. A magnification of the low-temperature region (Figure 7b) shows that this contribution nevertheless survives as indicated by the local maximum observed near 15 K. A further increase in x to 0.0015

then leads to a crossover from positive to negative values near 100 K. The negative sign remains unaffected down to 5 K and with increasing x to 0.0035. For these three compositions, a small maximum seems to be attained around 10 K, suggesting that the positive phonon-drag contribution is still present, albeit strongly reduced. Such a change from a dominant holelike to electronlike response suggests either the development of electron pockets with increasing x or a possible negative diffusion contribution to α. For x = 0.0045, the temperature range over which α is negative is reduced to below 60 K. Finally, positive values are recovered over the whole temperature range for $x \geq 0.01$. None of the samples show a linear temperature dependence characteristic of a diffusive regime, with the superlinear dependence observed below 200 K in the x = 0.01 sample being lessened in the x = 0.02 sample.

Figure 8 shows the temperature dependence of the total thermal conductivity κ. The x = 0.0 sample is characterized by a large room-temperature value of 7.8 W m^{-1} K^{-1} and a low-temperature Umklapp peak that reaches nearly 14 W m^{-1} K^{-1} at 35 K. While the overall shape of $\kappa(T)$ is only weakly affected by the substitution of In for Sn up to x = 0.02, increasing the In content results in a significant decrease in both the κ values and the magnitude of the Umklapp peak, which is nearly fully suppressed in the x = 0.07 sample. The overall evolution of its magnitude with x is consistent with enhanced point defect scattering that plays a prominent role in shaping the heat transport of SnTe at low temperatures.[44] The variations in κ with x are mainly due to the marked increase in the ρ values which strongly reduces the electronic contribution κ_e according to the Wiedemann-Franz relation $\kappa_e = LT/\rho$ where L is the Lorenz number.

C. Superconducting properties

The emergence of a superconducting state upon In doping has been investigated through specific heat (C_p) measurements between 0.35 and 4 K on the x = 0.0, 0.0035, 0.01, 0.02, 0.05 and 0.07 samples (Figure 9a). The electronic contribution to the normal-state specific heat γ_n was inferred from linear fits of the C_p/T data measured under zero magnetic field following the conventional relation $\frac{C_p}{T} = \gamma_n + \beta T^2 + \delta_2 T^4$, with the β and δ_2 terms accounting for the lattice contribution. This last term corresponds to the lowest order of the low-temperature expansion $\sum_{i=2}^{n} \delta_i T^{2i+1}$, usually used to better account for the non-linear temperature dependence of the lattice contribution beyond the β term. For all samples, the data were fitted between 0.12 and 4 K^2 for non-superconducting samples and above the superconducting transition and between 4 and 7 K^2 for $x \geq 0.02$ depending on T_c (Figure 9b). The fitted γ_n values vary between 0.18 for the x = 0.0 and a maximum of 0.84 mJ mol^{-1} K^{-2} achieved in the 0.05 sample. All these values are indicative of small densities of states at the Fermi level (see Table I), in agreement with those inferred from specific heat data measured on single-crystalline specimens.[47] The Debye temperatures θ_D, determined by the relation $\theta_D = \sqrt[3]{12\pi^4 NR/5\beta}$ where R is the ideal gas constant and N is the number of atoms per formula unit (here, $N = 2$ for all samples), tends to be lower in the In-containing samples (~ 172 K) compared to the value of the binary sample (185 K). This last high θ_D value may be a consequence of the small concentration of Sn vacancies in the In-free sample due to the Sn-rich conditions of the synthesis. In metals, θ_D has been linked to the vacancy formation energy E_V according to the relation $\theta_D = C \frac{\sqrt{E_V}}{\Omega^{1/3}\sqrt{M}}$ where C is a constant, M is the atomic mass and Ω is the atomic volume.[76,77] Samples with low vacancy concentrations are thus expected

to show higher θ_D values compared to more heavily-doped samples. As discussed below, the p_H data of the In-substituted samples do not corroborate the presence of a high concentration of vacancies that might explain the lower θ_D consistently observed over the entire In concentration range, suggesting that an additional lattice softening is induced by the substitution of In for Sn.

Upon cooling, well-defined superconducting transitions are observed for the x = 0.05 and 0.07 samples while a pronounced broadening in the transition occurs for x = 0.02. No superconducting transition is detected down to 0.35 K for x < 0.02. Using an equal entropy construction procedure, the critical temperatures T_c and normalized superconducting jumps $\Delta C_p/\gamma_n T_c$ were estimated to be 0.67 K, 1.34 K and 1.73 K and 1.01, 1.42 and 1.40 for the x = 0.02, 0.05 and 0.07 samples, respectively. Both the T_c values and the magnitudes of $\Delta C_p/\gamma T_c$ are consistent with those determined in prior studies on single crystals of $Sn_{1-\delta-x}In_xTe$ for similar substitution levels.[47-55] For x = 0.05 and 0.07, the values of $\Delta C_p/\gamma T_c$ are in reasonable agreement with the BCS, weak-coupling value of 1.43 suggesting that these samples can be classified as weakly-coupled superconductors.

Taking the θ_D and T_c values, the electron-phonon coupling constant λ_{el-ph} was estimated using the inverted McMillan formula[78]

$$\lambda_{el-ph} = \frac{1.04 + \mu^* \ln\left(\frac{\theta_D}{1.45T_c}\right)}{(1 - 0.62\mu^*)\ln\left(\frac{\theta_D}{1.45T_c}\right) - 1.04} \quad (1)$$

where μ^* is the Coulomb pseudopotential parameter, typically assumed to fall in the range 0.10 – 0.15. As the electronic densities of states are very low in this series, we assumed $\mu^* = 0.10$, resulting in λ_{el-ph} values of 0.41, 0.47 and 0.50 for the x = 0.02, 0.05 and 0.07 samples,

respectively, indicative of a weak coupling regime. From the values of $\lambda_{\mathrm{el-ph}}$ and γ, the noninteracting density of states at the Fermi level $N(E_{\mathrm{F}})$ was calculated from the equation

$$N(E_{\mathrm{F}}) = \frac{3\gamma}{\pi^2 k_B^2 (1 + \lambda_{\mathrm{el-ph}})} \quad (2)$$

yielding 0.16, 0.24 and 0.26 states per eV and per formula unit for the *x* = 0.02, 0.05 and 0.07 samples, respectively.

IV. Discussion

A. Influence of the RL on the normal-state transport properties

The presence of an In-induced RL provides a consistent picture that explains several traits observed in this series. The strong increase in the residual electrical resistivity ρ_0 with *x*, shown in Figure 10, reflects the significant drop in μ_H at 5 K by three orders of magnitude. This strong sensitivity to the In content is clearly beyond what may be expected from strain field effects and mass fluctuations induced by the substitution of In for Sn due to the small difference in molar mass. Of note, variations in the concentration of Sn vacancies, estimated to be around 0.0025 in the parent $Sn_{1.03}Te$ compound,[44] cannot account for the strong increase in ρ_0. Recent low-temperature transport property measurements on the binary SnTe prepared by various synthesis routes have shown that ρ_0 remains below 0.5 μΩ.m at 5 K despite variations in the vacancy concentration from 0.25 up to nearly 1.8%.[44] Although the presence of grain boundary scattering contributes to decrease μ_H, the strong effect observed is rather a natural consequence of enhanced scattering of holes by the RL, which strongly decreases their electronic lifetime, as indicated by the analysis of the Bloch spectral functions reported in our prior study.[67] Moreover, using the

Kubo-Greenwood formalism, a comparison of $\mu_H(T)$ data with various rigid-like and non-rigid-like, non-resonant impurities have shown that the impact of the In-induced RL on μ_H is a hallmark of resonant impurities, providing a simple and straightforward mean to discern the effect of an impurity on the electronic band structure of semiconductors.[67] Thus, the marked increase in ρ_0 as *x* increases supports the major role played by the RL on the low-temperature transport properties up to *x* = 0.05. As evidenced by our band structure calculations, increasing the In concentration above *x* = 0.02 widens the resonant DOS "hump", leading to a saturation of the resonant band smearing. The band smearing effect is maximized at *x* = 0.05, where the width of a single-point Bloch spectral function Δ (see Figure 2) reaches the L-Σ bandwidth. This explains the saturating tendency of $\rho_0(x)$ above *x* = 0.02, where Δ was already very large, with the maximum in $\rho_0(x)$ reached around 5%. Further increasing *x* leads to an enhanced hybridization and gradual resonance blurring, only slightly reducing the mobility. The estimation of the single-*k*-point relaxation time in Figure 1 showed a small decrease of τ between 0.05 and 0.07. However, this estimate of τ should be taken with caution since the Lorentzian function does not describe the shape of the spectral functions at these In concentrations (see Figure 2). To better quantify this effect, we have performed calculations of the electrical conductivity at *T* = 0 K using the Kubo-Greenwood formalism (see Ref. 67 for technical details and for calculations at lower In concentrations). These calculations yield ρ_0 values of 4.1 and 3.3 μΩ.m for *x* = 0.05 and 0.07, respectively, which compare well to the experimental values of 5.5 and 4.7 μΩ.m, respectively. The decrease in ρ_0 is due to the increase in carrier concentration between the *x* = 0.05 and 0.07 samples, accompanied by a small decrease in charge carrier mobility.

In agreement with prior studies,[22-44] the lower hole concentration achieved in the *x* = 0.0 sample, thanks to the initial Sn excess introduced, results in the emergence of the ferroelectric

transition at a higher temperature.[71-74] Although ARPES and quantum oscillation measurements have evidenced a reconstruction of the Fermi surface accompanying this transition,[75] it has little influence on the electrical and thermal properties and hence, does not affect the resonant nature of In.

From simple electron counting rules, In should behave as a hole dopant in $Sn_{1-\delta}Te$ due to its number of valence electrons with one fewer electron than Sn, that is, In^{1+} versus Sn^{2+}. Detailed investigations of the superconducting properties as a function of *x* between 0.05 and 0.40 revealed that a simple hole-doping picture only holds true up to about 0.09, a critical value above which the impact of In on the electronic band structure is too severe for a rigid-band-like shift of the chemical potential to be a consistent description of the system.[47-55] The non-rigid-like behavior above x = 0.09 further manifests in the Hall data with a crossover from a dominant holelike to electronlike response at 50 K.[53] For substitution levels lower than 0.09, the compounds remain *p*-type regardless of the In content with a good correlation between the In concentration and measured hole densities. Our experimental results support well this last conclusion with a hole-dopant behavior persisting across the entire doping range. As shown in Figure 11, where the hole density p_H as a function of *x* is presented, $p_H(x)$ increases quasi-linearly with *x*. For $x \geq 0.01$, a very good agreement is achieved between the experimental p_H values and the expected hole concentrations calculated by assuming that each In atom provides one hole (*i.e.* In^{1+} valence state). The slight but clear disagreement at lower doping levels likely reflects the concentration of Sn vacancies which progressively disappear as *x* increases. From these data, it seems reasonable to postulate that vacancies are no longer present beyond x = 0.01 or, at least, that their concentration is sufficiently low to have a negligible influence on the measured p_H. Thus, these results confirm that In behaves

as a hole dopant with a formal In^{1+} valence state, which constrains the possible amount of In^{3+} in this In concentration range.

While the increase in the room-temperature α values with the In content is consistent with the RL picture, evidenced by a strong departure of the $\alpha(p_H)$ dependence from the theoretical Ioffe-Pisarenko curve,[45,46,67] the non-monotonic evolution of α with x at low temperatures and, notably, the crossover from positive to negative values for $0.0015 \leq x \leq 0.0045$ is another intriguing aspect revealed by our experimental results. Several scenarios may be invoked to explain the overall trend in $\alpha(x,T)$ that include a charge-Kondo effect, a RL-induced effect or a phonon-drag contribution. The first scenario, a charge-Kondo effect, has been discussed in the series $Pb_{1-x}Tl_xTe$ (Ref. 17) for which the $\alpha(x,T)$ data are qualitatively similar to those obtained here for the series $Sn_{1.03-\delta-x}In_xTe$. In particular, a crossover from positive to negative α values below 100 K has been evidenced for a Tl content of 0.3%. Above this value, positive α values are recovered, which slightly increase with increasing x to 1.1% and eventually to 1.3%.[17] Because of these similarities between the two series, it is tempting to posit that $Sn_{1.03-x}In_xTe$ also harbors a charge-Kondo effect. However, this mechanism requires In in both In^{1+} and In^{3+} charge states, the presence of which is not supported by the Hall data.

The fact that both Tl and In act as resonant impurities suggests that the complex evolution of $\alpha(x,T)$ below 100 K may rather arise from band structure modifications induced by the RL. However, low-temperature measurements of α on the series $Pb_{0.99}Na_{0.01}Te_{1-x}S_x$ for x = 0.0, 0.04 and 0.12 have also evidenced a temperature region extending from 50 to 130 K over which α is negative.[76] In this series, neither Na nor S behave as resonant impurities showing that the presence of a RL is not a prerequisite to a positive-to-negative crossover in α. Furthermore, additional measurements under magnetic fields $\mu_0 H$ of up to 7T showed that positive values are progressively

recovered with increasing $\mu_0 H$. The overall $\alpha(\mu_0 H)$ evolution has been interpreted as a positive phonon-drag peak superimposed to a magnetic-field-dependent, negative diffusion contribution to α attributed to interband scattering between the valleys located at the L and Σ points of the BZ.[79] In the limit $\mu_0 H \rightarrow \infty$, $\alpha(\mu_0 H, T)$ becomes scattering independent,[80] explaining why positive α values are recovered at high magnetic fields.

To determine whether a similar dependence $\alpha(\mu_0 H)$ is observed in the series $Sn_{1.03-\delta-x}In_xTe$, α of the x = 0.0035 sample has been measured under magnetic fields of up to 14T (Figure 12). These data show that the temperature window over which $\alpha < 0$ is significantly reduced upon increasing $\mu_0 H$. In addition, the shape of $\alpha(T)$ is practically unaffected by the application of the magnetic field, as observed in $Pb_{0.99}Na_{0.01}Te_{1-x}S_x$ for x = 0.04.[79] The similar behavior of $\alpha(\mu_0 H)$ in these two series suggests that a negative diffusion contribution to α also exists in $Sn_{1.03-\delta-x}In_xTe$, which evolves with both the In concentration and, for a fixed x value, with $\mu_0 H$. The fact that α tends to positive values at high $\mu_0 H$ further indicates that the dominant charge carriers are holes, in agreement with the Hall data. The similar valence band structures of PbTe and SnTe, with notably valleys at the L and Σ points of the BZ, suggests that the negative diffusion thermopower in the latter may also originate from interband scattering. As an alternative scenario, electron pockets possibly emerging upon In substitution may undergo a strong Zeeman splitting effect, thereby progressively suppressing their contribution to α. This possibility has nevertheless been ruled out in Tl-doped PbTe and $Pb_{0.99}Na_{0.01}Te_{1-x}S_x$,[20,79] making a scattering-related effect more likely in In-doped SnTe.

B. Influence of the RL on superconductivity

In agreement with previous studies on single-crystalline and polycrystalline $Sn_{1-\delta-x}In_xTe$,[47-55] a superconducting state emerges upon In doping above a critical concentration that possibly falls between x = 0.01 and x = 0.02. The existence of this threshold is consistent with the estimate of 0.017 deduced from transport and thermodynamic data in single-crystalline specimens.[47] The x-dependence of the critical temperature T_c follows the reported general trend with a nearly linear increase in T_c for In contents of up to 0.09 followed by a weaker dependence up to x = 0.50 (Figure 13).

The evolution of the magnitude of the electronic contribution to the normal-state specific heat γ_n with the hole concentration p_H measured at 5 K is consistent with the development of a RL near the top of the valence band manifold. The comparison of the γ_n values of the In-substituted samples with that measured for $Sn_{1.03}Te$ ($\gamma_n = 0.18$ mJ mol^{-1} K^{-2} for 9.2×10^{19} cm^{-3} at 5 K) indicates that the presence of In tends to give rise to enhanced γ_n values (between 0.39 and 0.55 mJ mol^{-1} K^{-2} for x = 0.0035 and 0.02, respectively, and for p_H varying between 2.17×10^{20} and 4.5×10^{20} cm^{-3} at 5 K, respectively). Noteworthy is the fact that a direct comparison with the values measured for In-free samples $Sn_{1-\delta}Te$ with $\delta > 0.0025$ is complicated by the second, heavy-hole valence band that starts to contribute above ~2×10^{20} cm^{-3} resulting in a rapid increase in γ_n up to 1.5 mJ mol^{-1} K^{-2} for $\delta \sim 0.035$ (corresponding to $p_H \sim 1.66\times10^{21}$ cm^{-3} at 5 K).[22,27,44] Upon In doping, the enhancement in γ_n is qualitatively consistent with our calculations predicting an increase in $N(E_F)$. However, the electron-phonon interactions present in all of the studied samples, which may be responsible for superconductivity, additionally enhance the electronic specific heat over the pure band structure values, $\gamma_n = \gamma_{band}(1 + \lambda_{el-ph})$, complicating the analysis and direct comparison

with calculations. As already mentioned, assuming that superconductivity observed for $x \geq 0.02$ is due to electron-phonon interactions, we may use the λ_{el-ph} estimated from the McMillan formula (Eq.1) to calculate the non-interacting $N(E_{\mathrm{F}})_{exp}$ values with Eq.(2) and compare them to our DFT results (see Table I). For the non-superconducting samples, $\lambda_{el-ph} = 0$ was assumed, giving an upper bound for $N(E_{\mathrm{F}})$. Taking into account how relatively small the values of $N(E_{\mathrm{F}})$ are, qualitative agreement is found, but the computed values are visibly overestimated. The reason behind this issue is most likely the well-known problem faced by DFT calculations for Pb- and Sn-based chalcogenides, which is related to inaccuracy of the local-density approximation in reproducing the shape of the valence band at the L and between the L and Σ points of the BZ. The LDA band at the L point is too flat, and the energy separation between the two band maxima at the L and Σ points is too small, which leads to several disagreements between calculations and experiments. Among them, we may list an overestimated DOS effective mass in SnTe:In (Ref. 46) and PbTe:Tl (Ref. 13) as well as a widely-discussed problem of an overestimation of the computed thermopower of *p*-type PbTe.[13,81] This local-density inaccuracy is directly related to the computed too large $N(E_{\mathrm{F}})$ values. Of note, if we assume that the electron-phonon interaction is responsible for superconductivity in SnTe:In, the λ_{el-ph} values inferred from the McMillan formula should be considered as reliable, as all the samples of this series are in the adiabatic regime where the condition $\hbar\omega_D \ll E_F$ prevails (ω_D is the Debye frequency).[82] Based on our calculations, E_F is found to increase from 130 meV for $x = 0.005$ (with Sn vacancies) to 250 meV for $x = 0.07$, while $\hbar\omega_D$ remains on the order of 15 meV across the entire substitution range. The fact that this condition is fulfilled ensures that all corrections small in $\hbar\omega_D/E_F$ can be safely neglected by Migdal's theorem,[76,82] one of the prerequisite the McMillan formula is based on. Here, the inaccuracy of LDA in predicting E_F is not a threat to meeting the above-mentioned criterion, as

the "true" band structure with smaller density-of-states effective mass and $N(E_F)$ will have larger E_F at the same hole concentration. Thus, our LDA estimates of the Fermi energy can be considered as lower bounds, further ensuring that the above-mentioned condition is not compromised.

Intriguingly, our results further confirm the anomalous evolution of the normalized specific heat jump $\Delta C_p/\gamma T_c$ with x, which significantly broadens as the In concentration is lowered. While the polycrystalline nature of this sample may provide a natural explanation for the absence of a sharp transition, similar results were reported on single-crystalline samples of $Sn_{1-\delta-x}In_xTe$ and $Pb_{1-x}Tl_xTe$,[19,47] demonstrating that this broadening is independent of the nature of the samples. Inhomogeneities in the spatial distribution of In has been proposed as a possible origin of this behavior.[47] However, our TEM analyses carried out on the x = 0.02 sample did not evidence any significant inhomogeneity in the spatial distribution of In in this sample, suggesting that this behavior is an intrinsic property of RL-containing superconductors.

All these results, that closely parallel those reported in $Pb_{1-x}Tl_xTe$,[12-21] naturally raise the question of the driving mechanism behind the enhanced T_c values observed upon In doping. A first possibility is related to the ferroelectric structural phase transition observed in the $\rho(T)$ data at low temperatures that persists upon In doping. In $Sn_{1-\delta}Te$, this structural instability is connected to the lowest-energy transverse optical phonon mode that softens upon cooling to nearly zero energy at T_{SPT}, before hardening as the temperature is further decreased below T_{SPT}.[74] The coupling between this soft polar optical phonon mode and charge carriers has been suggested to play a key role in enhancing the electron-phonon coupling and hence, T_c, in several ferroelectric compounds.[83-85] However, our results confirm the linear decrease in the transition temperature T_{SPT} with increasing p_H and the lack of correlation with T_c reported previously,[47] suggesting that the ferroelectric instability plays a secondary role in determining T_c in $Sn_{1-\delta-x}In_xTe$.

A second mechanism proposed to explain the observed trends in the superconducting properties with x is related to a mixed-valence scenario for which fluctuations between +1 and +3 In valence states would be required.[15-18,47] These two valence states, when degenerate, may be associated to a charge Kondo effect that would provide both a pairing mechanism with variations in the pairing interaction V with x and a source of DOS enhancement related to Kondo physics. Although the tendency for In to skip a +2 valence state has been observed in several In-containing compounds,[56,57] the variation in p_H with x can be well explained by considering the presence of only In^{+1} cations in addition to a small amount of Sn vacancies that seem to be progressively removed with increasing the In content. In this regard, further x-ray photoelectron spectroscopy would be worthwhile to provide experimental evidence or rule out a mixed-valence scenario in $Sn_{1-\delta-x}In_xTe$.

In contrast to these exotic mechanisms, a phonon-mediated pairing interaction varying with the In concentration may provide a more mundane explanation. The development of the RL might selectively enhance some electron-phonon coupling matrix elements, explaining the higher-than-expected T_c values observed in RL-containing superconductors. However, the exact role played by the In-induced RL on the phonon- and electron-momentum dependence of the electron-phonon coupling is yet to be fully understood. Although computationally-demanding, detailed calculations of this coupling taken into account the smearing of the valence bands induced by the RL would be helpful to elucidate the origin of the apparent anomalies in the superconducting parameters found in RL-containing superconductors.

V. Summary and conclusion

We have reported a detailed investigation of the evolution of the normal-state and superconducting properties of the series $Sn_{1.03-\delta-x}In_xTe$ for doping levels spanning a wide range of In concentrations from 0.5% up to 7%. Even though most of the substitution levels probed herein are very low, the results reveal a strong sensitivity of the transport and superconducting properties to the In concentration. The main characteristics of the variations with x can be well explained within an In-induced resonant-level scenario, conforming to the main predictions of our electronic band structure calculations. Our results notably evidence a complex evolution of the low-temperature thermopower with x. A crossover from positive to negative values that sets in near 100 K exists over the narrow In concentration range $0.0015 \leq x \leq 0.0045$. The magnetic field dependence of $\alpha(\mu_0 H)$, measured for the x = 0.0035 sample, nevertheless suggests a dominant holelike response, as indicated by the progressive shift of α towards positive values with increasing $\mu_0 H$. The presence of negative α values over restricted temperature and compositional ranges are strikingly similar to those observed in Tl-doped PbTe. However, unlike $Pb_{1-x}Tl_xTe$ where the disproportionation of Tl into Tl^{1+} and Tl^{3+} has received experimental support, the x dependence of the carrier concentration suggests that In behaves as a hole dopant. The development of the RL is accompanied by the emergence of superconductivity, detectable for $x \geq 0.02$ above 0.35 K, with a critical temperature increasing with x to reach 1.73 K for x = 0.07. While the BCS theory provides a relevant framework to understand qualitatively the observed trends in the superconducting parameters, some experimental evidences hint at a non-trivial enhancement of the phonon-mediated pairing strength with x that is likely induced by the formation of the RL. Whether this mechanism applies to the present series and can be generalized to other RL-containing

superconductors will require further detailed calculations of the electron-phonon coupling. All these results show that the series $Sn_{1.03-\delta-x}In_xTe$ provides another valuable system where the interplay between RL-induced enhanced thermopower and superconductivity can be systematically investigated.

Acknowledgments

B. W. was supported by the National Science Centre (Poland), project No. 2017/26/E/ST3/00119. P. L. and J. H. acknowledge the financial support of the Czech Science Foundation (project 18-12761S). Experiments were performed in MGML (mgml.eu), which is supported within the program of Czech Research Infrastructures (project no. LM2018096).

References

[1] Goldsmid, H. J. in *Thermoelectric Refrigeration*; Springer: New York, 1964.

[2] Thermoelectrics and its Energy Harvesting, edited by D. M. Rowe (CRC Press, 2012).

[3] J. P. Heremans, V. Jovovic, E. S. Toberer, A. Saramat, K. Kurosaki, A. Charoenphakdee, S. Yamanaka and G. J. Snyder, Enhancement of thermoelectric efficiency in PbTe by distortion of the electronic density of states, Science **321**, 554–557 (2008).

[4] D. G. Mahan and J. O. Sofo, The best thermoelectric, Proc. Natl. Acad. Sci. U.S.A. **93**, 7436–7439 (1996).

[5] J. P. Heremans, B. Wiendlocha and A. M. Chamoire, Resonant levels in bulk thermoelectric semiconductors, Energy Environ. Sci. **5**, 5510–5530 (2012).

[6] B. Wiendlocha, Localization and magnetism of the resonant impurity states in Ti doped PbTe, Appl. Phys. Lett. **105**, 133901 (2014).

[7] C. M. Jaworski, V. Kulbachinskii and J. P. Heremans, Resonant level formed by tin in Bi_2Te_3 and the enhancement of room-temperature thermoelectric power, Phys. Rev. B **80**, 233201 (2009).

[8] B. Wiendlocha, Resonant Levels, Vacancies, and Doping in Bi_2Te_3, Bi_2Te_2Se, and Bi_2Se_3 Tetradymites, J. Electron. Mater. **45**, 3515–3531 (2016).

[9] B. Wiendlocha, J.-B. Vaney, C. Candolfi, A. Dauscher, B. Lenoir and J. Tobola, An Sn-induced resonant level in β-As_2Te_3, Phys. Chem. Chem. Phys. **20**, 12948–12957 (2018).

[10] L. Whu, X. Li, S. Wang, T. Zhang, J. Yang, W. Zhang, L. Chen and J. Yang, Resonant level-induced high thermoelectric response in indium-doped GeTe, NPG Asia Mater. **9**, e343 (2017).

[11] S. A. Nemov and Y. I. Ravich, Thallium dopant in lead chalcogenides: investigation methods and peculiarities, Sov. Phys. Usp. **41**, 735 (1998).

[12] V. I. Kaidanov and Y. I. Ravich, Deep and resonance states in A^{IV} B^{VI} semiconductors, Sov. Phys. Usp. **28**, 31 (1985).

[13] B. Wiendlocha, Thermopower of thermoelectric materials with resonant levels: PbTe:Tl versus PbTe:Na and $Cu_{1-x}Ni_x$, Phys. Rev. B **97**, 205203 (2018).

[14] M. Dzero and J. Schmalian, Superconductivity in Charge Kondo Systems, Phys. Rev. Lett. **94**, 157003 (2005).

[15] H. Matsuura and K. Miyake, Theory of Charge Kondo Effect on Pair Hopping Mechanism, J. Phys. Soc. Jpn. **81**, 113705 (2012).

[16] T. A. Costi and V. Zlatić, Charge Kondo Anomalies in PbTe Doped with Tl Impurities, Phys. Rev. Lett. **108**, 036402 (2012).

[17] M. Matusiak, E. M. Tunnicliffe, J. R. Cooper, Y. Matsushita and I. R. Fisher, Evidence for a charge Kondo effect in $Pb_{1-x}Tl_xTe$ from measurements of thermoelectric power, Phys. Rev. B **80**, 220403 (2009).

[18] Y. Matsushita, H. Bluhm, T. H. Geballe, and I. R. Fisher, Evidence for Charge Kondo Effect in Superconducting Tl-Doped PbTe, Phys. Rev. Lett. **94**, 157002 (2005).

[19] Y. Matsushita, P. A.Wianecki, A. T. Sommer, T. H. Geballe, and I. R. Fisher, Type II superconducting parameters of Tl-doped PbTe determined from heat capacity and electronic transport measurements, Phys. Rev. B **74**, 134512 (2006).

[20] P. Giraldo-Gallo, P. Walmsley, B. Sangiorgio, S. C. Riggs, R. D. MacDonald, L. Buchauer, B. Fauqué, C. Liu, N. A. Spaldin, A. Kaminski, K. Behnia and I. R. Fisher, Evidence of incoherent carriers associated with resonant impurity levels and their influence on superconductivity in the anomalous superconductor $Pb_{1-x}Tl_xTe$, Phys. Rev. Lett. **121**, 207001 (2018).

[21] P. Walmsley, D. Palczewski, P. Giraldo-Gallo, C. G. Olson, I. R. Fisher and A. Kaminski, Direct spectroscopic evidence for mixed-valence Tl in the low carrier-density superconductor $Pb_{1-x}Tl_xTe$, Phys. Rev. B **98**, 184506 (2018).

[22] G. Tan, L-D. Zhao, F. Shi, J. W. Doak, S.-H. Lo, H. Sun, P. Wang, C. Wolverton, V. P. Dravid, C. Uher, and M. G. Kanatzidis, High thermoelectric performance of p-type SnTe via a synergistic band engineering and nanostructuring approach, J. Am. Chem. Soc. **136**, 7006–7017 (2014).

[23] G. Tan, F. Shi, S. Hao, H. Chi, L-D. Zhao, C. Uher, C. Wolverton, V. P. Dravid, and M. G. Kanatzidis, Codoping in SnTe: Enhancement of Thermoelectric Performance through Synergy of Resonance Levels and Band Convergence, J. Am. Chem. Soc. **137**, 5100–5112 (2015).

[24] G. Tan, F. Shi, S. Hao, H. Chi, T. P. Bailey, L-D. Zhao, C. Uher, C. Wolverton, V. P. Dravid, and M. G. Kanatzidis, Valence Band Modification and High Thermoelectric Performance in SnTe Heavily Alloyed with MnTe, J. Am. Chem. Soc. **137**, 11507–11516 (2015).

[25] G. Tan, F. Shi, J. W. Doak, H. Sun, L-D. Zhao, P. Wang, C. Uher, C. Wolverton, V. P. Dravid and M. G. Kanatzidis, Extraordinary role of Hg in enhancing the thermoelectric performance of *p*-type SnTe, Energy Environ. Sci. **8**, 267–277 (2015).

[26] G. Tan, W. G. Zeier, F. Shi, P. Wang, G. J. Snyder, V. P. Dravid, and M. G. Kanatzidis, High Thermoelectric Performance SnTe–In_2Te_3 Solid Solutions Enabled by Resonant Levels and Strong Vacancy Phonon Scattering, Chem. Mater. **27**, 7801–7811 (2015).

[27] M. Zhou, Z. M. Gibbs, H. Wang, Y. Han, C. Xin, L. Li and G. J. Snyder, Optimization of thermoelectric efficiency in SnTe: the case for the light band, Phys. Chem. Chem. Phys. **16**, 20741–20748 (2014).

[28] J. He, X. Tan, J. Xu, G.-Q. Liu, H. Shao, Y. Fu, X. Wang, Z. Liu, J. Xu, H. Jiang and J. Jiang, Valence band engineering and thermoelectric performance optimization in SnTe by Mn-alloying

via a zone-melting method, J. Mater. Chem. A **3**, 19974–19979 (2015).

[29] A. Banik, U. S. Shenoy, S. Anand, U. W. Waghmare and K. Biswas, Mg Alloying in SnTe Facilitates Valence Band Convergence and Optimizes Thermoelectric Properties, Chem. Mater. **27**, 581–587 (2015).

[30] Z. Zhou, J. Yang, Q. Jiang, Y. Luo, D. Zhang, Y. Ren, X. He and J. Xin, Multiple effects of Bi doping in enhancing the thermoelectric properties of SnTe, J. Mater. Chem. A **4**, 13171–13175 (2016).

[31] L-D. Zhao, X. Zhang, H. Wu, G. Tan, Y. Pei, Y. Xiao, C. Chang, D. Wu, H. Chi, L. Zheng, S. Gong, C. Uher, J. He and M. G. Kanatzidis, Enhanced Thermoelectric Properties in the Counter-Doped SnTe System with Strained Endotaxial SrTe, J. Am. Chem. Soc. **138**, 2366–2373 (2016).

[32] R. Al Rahal Al Orabi, J. Hwang, C.-C. Lin, R. Gautier, B. Fontaine, W. Kim, J.-S. Rhyee, D. Wee and M. Fornari, Ultralow Lattice Thermal Conductivity and Enhanced Thermoelectric Performance in SnTe:Ga Materials, Chem. Mater. **29**, 612–620 (2017).

[33] L. Zhang, J. Wang, Z. Cheng, Q. Sun, Z. Li and S. Dou, Lead-free SnTe-based thermoelectrics: enhancement of thermoelectric performance by doping with Gd/Ag, J. Mater. Chem. A **4**, 7936–7942 (2016).

[34] A. Banik, B. Vishal, S. Perumal, R. Datta and K. Biswas, The origin of low thermal conductivity in $Sn_{1-x}Sb_xTe$: phonon scattering via layered intergrowth nanostructures, Energy Environ. Sci. **9**, 2011–2019 (2016).

[35] R. Al Rahal Al Orabi, N. A. Mecholsky, J. Hwang, W. Kim, J.-S. Rhyee, D. Wee and M. Fornari, Band Degeneracy, Low Thermal Conductivity, and High Thermoelectric Figure of Merit in SnTe–CaTe Alloys, Chem. Mater. **28**, 376–384 (2016).

[36] L. Wang, X. Tan, G. Liu, J. Xu, H. Shao, B. Yu, H. Jiang, S. Yue and J. Jiang, Manipulating Band Convergence and Resonant State in Thermoelectric Material SnTe by Mn–In Codoping, ACS Energy Lett. **2**, 1203–1207 (2017).

[37] W. Li, L. Zheng, B. Ge, S. Lin, X. Zhang, Z. Chen, Y. Chang and Y. Pei, Promoting SnTe as an Eco-Friendly Solution for p-PbTe Thermoelectric via Band Convergence and Interstitial Defects, Adv. Mater. **29**, 1605887 (2017).

[38] N. Wang, D. West, J. Liu, J. Li, Q. Yan, B.-L. Gu, S. B. Zhang and W. Duan, Microscopic origin of the *p*-type conductivity of the topological crystalline insulator SnTe and the effect of Pb alloying, Phys. Rev. B **89**, 045142 (2014).

[39] L. Zheng, W. Li, S. Lin, J. Li, Z. Chen and Y. Pei, Interstitial Defects Improving Thermoelectric SnTe in Addition to Band Convergence, ACS Energy Lett. **2**, 563–568 (2017).

[40] L. Hu, Y. Zhang, H. Wu, J. Li, Y. Li, M. McKenna, J. He, F. Liu, S. J. Pennycook and X. Zeng, Entropy Engineering of SnTe: Multi-Principal-Element Alloying Leading to Ultralow Lattice Thermal Conductivity and State-of-the-Art Thermoelectric Performance, Adv. Energy Mater. **8**, 1802116 (2018).

[41] J. Q. Li, S. Huang, Z. P. Chen, Y. Li, S. H. Song, F. S. Liu and W. Q. Ao, Phases and thermoelectric properties of SnTe with (Ge, Mn) co-doping, Phys. Chem. Chem. Phys. **19**, 28749–28755 (2017).

[42] S. Roychowdhury, U. S. Shenoy, U. V. Waghmare and K. Biswas, An enhanced Seebeck coefficient and high thermoelectric performance in p-type In and Mg co-doped $Sn_{1-x}Pb_xTe$ via the co-adjuvant effect of the resonance level and heavy hole valence band, J. Mater. Chem. C **5**, 5737–5748 (2017).

[43] D. Ibrahim, V. Ohorodniichuk, C. Candolfi, C. Semprimoschnig, A. Dauscher and B. Lenoir, Improved Thermoelectric Properties in Melt-Spun SnTe, ACS Omega **2**, 7106–7111 (2017).

[44] D. Ibrahim, C. Candolfi, S. Migot, J. Ghanbaja, A. Dauscher, B. Malaman, C. Semprimoschnig and B. Lenoir, Comprehensive study of the low-temperature transport properties of polycrystalline $Sn_{1+x}Te$ (x = 0 and 0.03), Phys. Rev. Mater. **3**, 085404 (2019).

[45] Q. Zhang, B. Liao, Y. Lan, K. Lukas, W. Liu, K. Esfarjani, C. Opeil, D. Broido, G. Chen and Z. Ren, Proc. Natl. Acad. Sci. U.S.A. **110**, 13261–13266 (2013).

[46] S. Misra, B. Wiendlocha, J. Tobola, F. Fesquet, A. Dauscher, B. Lenoir and C. Candolfi, Band structure engineering in $Sn_{1.03}Te$ through an In-induced resonant level, J. Mater. Chem. C **8**, 977 (2020).

[47] A. S. Erickson, J.-H. Chu, M. F. Toney, T. H. Geballe and I. R. Fisher, Enhanced superconducting pairing interaction in indium-doped tin telluride, Phys. Rev. B **79**, 024520 (2019).

[48] P. B. Allen and M. L. Cohen, Carrier-Concentration-Dependent Superconductivity in SnTe and GeTe, Phys. Rev. **177**, 704 (1969).

[49] G. S. Bushmarina, I. A. Drabkin, V. V. Kompaniets, R. V. Parfen'ev, D. V. Shamshur, and M. A. Shakhov, Sov. Phys. Solid State **28**, 612 (1986).

[50] T. H. Hsieh, H. Lin, J. Liu, W. Duan, A. Bansil and L. Fu, Nat. Commun. **3**, 982 (2012).

[51] Y. Tanaka, Z. Ren, T. Sato, K. Nakayama, S. Souma, T. Takahashi, K. Segawa and Y. Ando, Nat. Phys. **8**, 800 (2012).

[52] S. Sasaki, Z. Ren, A. A. Taskin, K. Segawa, L. Fu and Y. Ando, Phys. Rev. Lett. **109**, 217004 (2012).

[53] N. Haldolaarachchige, Q. Gibson, W. Xie, M. B. Nielsen, S. Kushwaha and R. J. Cava, Anomalous composition dependence of the superconductivity in In-doped SnTe, Phys. Rev. B **93**, 024520 (2016).

[54] R. D. Zhong, J. A. Schneeloch, X. Y. Shi, Z. J. Xu, C. Zhang, J. M. Tranquada, Q. Li and G. D. Gu, Optimizing the superconducting transition temperature and upper critical field of $Sn_{1-x}In_xTe$, Phys. Rev. B **88**, 020505 (2013).

[55] G. Balakrishnan, L. Bawden, S. Cavendish and M. R. Lees, Superconducting properties of the In-substituted topological crystalline insulator SnTe, Phys. Rev. B **87**, 140507 (2013).

[56] J. A. J. Pardoe and A. J. Downs, Development of the Chemistry of Indium in Formal Oxidation States Lower than +3, Chem. Rev. **107**, 2 – 45 (2007).

[57] C.-J. Kang and G. Kotliar, Material design of indium-based compounds: Possible candidates for charge, valence, and bond disproportionation and superconductivity, Phys. Rev. Mater. **3**, 015001 (2019).

[58] H. Ebert, D. Ködderitzsch, J. Minár, Calculating condensed matter properties using the KKR-Green's function method—recent developments and applications, Rep. Prog. Phys. **74**, 096501 (2011).

[59] H. Ebert et al., The Munich SPR-KKR package, version 7.7.3, https://www.ebert.cup.uni-muenchen.de/index.php/en/software-en/13-sprkkr (2019)].

[60] S. H. Vosko, L. Wilk and M. Nusair, Accurate Spin-Dependent Electron Liquid Correlation Energies for Local Spin Density Calculations: A Critical Analysis, Can. J. Phys. **58**, 1200 (1980).

[61] P. Lloyd, Wave propagation through an assembly of spheres: II. The density of single-particle eigenstates, Proc. Phys. Soc. London **90**, 207 (1967).

[62] R. Kubo, Statistical-Mechanical Theory of Irreversible Processes. I. General Theory and Simple Applications to Magnetic and Conduction Problems, J. Phys. Soc. Jpn. **12**, 570 (1957).

[63] D. A. Greenwood, The Boltzmann Equation in the Theory of Electrical Conduction in Metals, Proc. Phys. Soc. **71**, 585 (1958).

[64] W. H. Butler, Theory of electronic transport in random alloys: Korringa-Kohn-Rostoker coherent-potential approximation, Phys. Rev. B **31**, 3260 (1985).

[65] T. Sato, Y. Tanaka, K. Nakayama, S. Souma, T. Takahashi, S. Sasaki, Z. Ren, A. A. Taskin, K. Segawa and Y. Ando, Fermiology of the Strongly Spin-Orbit Coupled Superconductor $Sn_{1-x}In_xTe$: Implications for Topological Superconductivity, Phys. Rev. Lett. **110**, 206804 (2013).

[66] J. S. Faulkner and G. M. Stocks, Calculating properties with the coherent-potential approximation, Phys. Rev. B **21**, 3222 (1980).

[67] B. Wiendlocha, S. Misra, A. Dauscher, B. Lenoir and C. Candolfi, Residual resistivity as an independent indicator of resonant levels in semiconductors, Mater. Horiz. **8**, 1735 (2021).

[68] R. F. Brebrick and A. J. Strauss, Anomalous Thermoelectric Power as Evidence for Two-Valence Bands in SnTe, Phys. Rev. **131**, 104 (1963).

[69] R. F. Brebrick, Deviations from stoichiometry and electrical properties in SnTe, J. Phys. Chem. Solids **24**, 27 (1963).

[70] J. A. Kafalas, R. F. Brebrick, and A. J. Strauss, Evidence that SnTe is a semiconductor, Appl. Phys. Lett. **4**, 93 (1964).

[71] K. Kobayashi, Y. Kato, Y. Katayama, and K. Komatsubara, Carrier-Concentration-Dependent Phase Transition in SnTe, Phys. Rev. Lett. **37**, 772 (1976).

[72] P. Littlewood, The crystal structure of IV-VI compounds. I. Classification and description, J. Phys. C **13**, 4875 (1980).

[73] P. Littlewood, The crystal structure of IV-VI compounds. II. A microscopic model for cubic/rhombohedral materials, J. Phys. C **13**, 4855 (1980).

[74] C. D. O'Neill, D. A. Sokolov, A. Hermann, A. Bosak, C. Stock and A. D. Huxley, Inelastic x-ray investigation of the ferroelectric transition in SnTe, Phys. Rev. B **95**, 144101 (2017).

[75] C. D. O'Neill, O. J. Clark, H. D. J. Keen, F. Mazzola, I. Markovic, D. A. Sokolov, A. Malekos, P. D. C. King, A. Hermann and A. D. Huxley, Changes of Fermi surface topology due to the rhombohedral distortion in SnTe, Phys. Rev. B **102**, 155132 (2020).

[76] K. Mukherjee, Monovacancy formation energy and Debye temperature of closepacked metals, Philos. Mag. **12**, 915–918 (1965).

[77] N. H. March, Vacancy formation energy and Debye temperature in close packed metals, Phys. Lett. **20**, 231–232 (1966).

[78] W. L. McMillan, Transition temperature of strong-coupled superconductors, Phys. Rev. **167**, 331 (1968).

[79] C. M. Jaworski, M. D. Nielsen, H. Wang, S. N. Girard, W. Cai, W. D. Porter, M. G. Kanatzidis and J. P. Heremans, Valence-band structure of highly efficient *p*-type thermoelectric PbTe-PbS alloys, Phys. Rev. B **87**, 045203 (2013).

[80] Y. I. Ravich, *Semiconducting Lead Chalcogenides* (Plenum Press, New York, NY, 1979).

[81] K. Berland and C. Persson, Thermoelectric transport of GaAs, InP, and PbTe: Hybrid functional with $k.\tilde{p}$ interpolation versus scissor-corrected generalized gradient approximation, J. Appl. Phys. **123**, 205703 (2018).

[82] A. B. Migdal, Interaction between electrons and lattice vibrations in a normal metal, Sov. Phys. JETP **7**, 996 (1958).

[83] J. Ma, R. Yang and H. Chen, A large modulation of electron-phonon coupling and an emergent superconducting dome in doped strong ferroelectrics, Nat. Commun. **12**, 2314 (2021).

[84] X. Lin, Z. Zhu, B. Fauqué, and K. Behnia, Fermi surface of the most dilute superconductor. Phys. Rev. X **3**, 021002 (2013).

[85] D. van der Marel, F. Barantani, and C. W. Rischau, Possible mechanism for superconductivity in doped $SrTiO_3$. Phys. Rev. Res. **1**, 013003 (2019).

Tables

Table I. Experimental values of the Sommerfeld coefficient $\gamma_{n,exp}$, Debye temperature θ_D, electron-phonon coupling parameter λ_{el-ph} and density of states at the Fermi level $N(E_\mathrm{F})_{exp}$ (Eq.2) compared to the computed values $N(E_\mathrm{F})_{calc}$.

x	p_H (cm^{-3})	$\gamma_{n,exp}$ (mJ mol^{-1} K^{-2})	θ_D (K)	λ_{el-ph}	$N(E_\mathrm{F})_{exp}$ (eV^{-1})	$N(E_\mathrm{F})_{calc}$ (eV^{-1})
0	1.04×10^{20}	0.18	185	/	0.08*	0.13
0.0035	2.17×10^{20}	0.39	170	/	0.17*	0.18
0.02	4.51×10^{20}	0.55	173	0.41	0.17	0.25
0.05	8.10×10^{20}	0.84	171	0.47	0.24	0.34
0.07	1.50×10^{21}	0.65	172	0.50	0.18	0.42

* computed assuming $\lambda_{el-ph} = 0$

Figure captions

FIG. 1. Calculated Bloch spectral density functions (BSF) and densities of states (DOS) for SnTe containing: (a) 0.32% of Sn vacancies; (b) 2% of In on Sn site; (c) 5% of In on Sn site; (d) 7% of In on Sn site. BSFs (left panels) are plotted for a selected *k*-path between the Γ, L and Σ points in the Brillouin zone, in a logarithmic scale (the color represents the BSF values in atomic units). In DOS plots (right panels), the total DOS is given per formula unit, while the partial In DOS is given per impurity atom (*i.e.* not multiplied by its concentration). The saturation of the band smearing effect for the larger In content to the whole L-Σ band is well visible and explains the experimentally observed evolution in electrical resistivity. The marked k_s point, located between L and Σ, is selected as a representative point to draw a single-point BSF in Figure 2.

FIG. 2. Points show the calculated Bloch spectral function BSF at k_s point (see Figure 1) for SnTe containing: (a) 0.32% of Sn vacancies; (b) 2% of In on Sn site; (c) 5% of In on Sn site; (d) 7% of In on Sn site, while the solid line is a fit to the Lorenz function. Carrier lifetime is estimated from the full width at half maximum Δ of the fitted Lorentzian as $\tau = \hbar/\Delta$. The fit is very good for a non-resonant Vac_{Sn} and fails for a resonant In_{Sn} doping. Thus, τ is only a rough estimate. The value of Δ becomes as large as the L-Σ bandwidth, naturally explaining the saturation in the residual electrical resistivity.

FIG. 3. Powder x-ray diffraction patterns of the series $Sn_{1.03-\delta-x}In_xTe$ for $0 \leq x \leq 0.07$. The asterisks mark the positions of additional reflections of elemental Sn. Their absence on the patterns of the $x = 0.05$ and $x = 0.07$ samples is due to the lack of Sn excess during the synthesis of these two samples.

FIG. 4. a) Low-magnification bright-field (BF) image with the corresponding EDS mappings of b) Sn, c) Te and d) In.

FIG. 5. (a) Temperature dependence of the electrical resistivity ρ for the series $Sn_{1.03-\delta-x}In_xTe$ ($0 \leq x \leq 0.07$). b) Temperature dependence of ρ normalized to the room-temperature value ρ_{300K}. The change in slopes around 100 K is due to the ferroelectric transition. In both panels, the solid lines are guides to the eye.

FIG. 6. a) Room-temperature transverse electrical resistivity ρ_{xy} as a function of the magnetic field $\mu_0 H$ for the illustrative samples $x = 0$, 0.0035, 0.02 and 0.07. The solid lines are guides to the eye. b) Temperature dependence of the hole concentration p_H for the series $Sn_{1.03-\delta-x}In_xTe$. c) Hall mobility μ_H as a function of temperature. In both panels, the solid lines are guides to the eye.

FIG. 7. a) Temperature dependence of the thermopower α for the series $Sn_{1.03-\delta-x}In_xTe$. b) Magnification of the low-temperature region where the transition from *p* to *n*-type α values occurs for $0.0015 \leq x \leq 0.0045$.

FIG. 8. Temperature dependence of the total thermal conductivity κ for the series $Sn_{1.03-\delta-x}In_xTe$.

FIG. 9. a) Specific heat data plotted as C_p/T versus T for the x = 0, 0.0035, 0.01, 0.02, 0.05 and 0.07 samples evidencing the superconducting transition that develops for $x \geq 0.02$. b) C_p/T as a function of T^2 for the illustrative x = 0, 0.0035 and 0.02 samples. The black dashed lines stand for the best fits to the data according to the polynomial expansion presented in the text.

FIG. 10. Residual electrical resistivity ρ_0 as a function of the In concentration x. The solid lines are guides to the eye.

FIG. 11. Hole concentration p_H as a function of the In concentration x. The solid black line is a guide to the eye. The solid red line represents the expected variations in the hole concentration p_H assuming a In^{1+} valence state.

FIG. 12. Temperature dependence of the thermopower α of the x = 0.0035 sample under magnetic fields $\mu_0 H$ of 0, 4, 7, 10 and 14 T. The black arrow shows the overall evolution of α with increasing $\mu_0 H$.

FIG. 13. Superconducting transition temperature T_c as a function of the In content x. For comparison purposes, selected data reported in prior studies across the entire homogeneity range have been added (Refs. 47, 53 and 54).

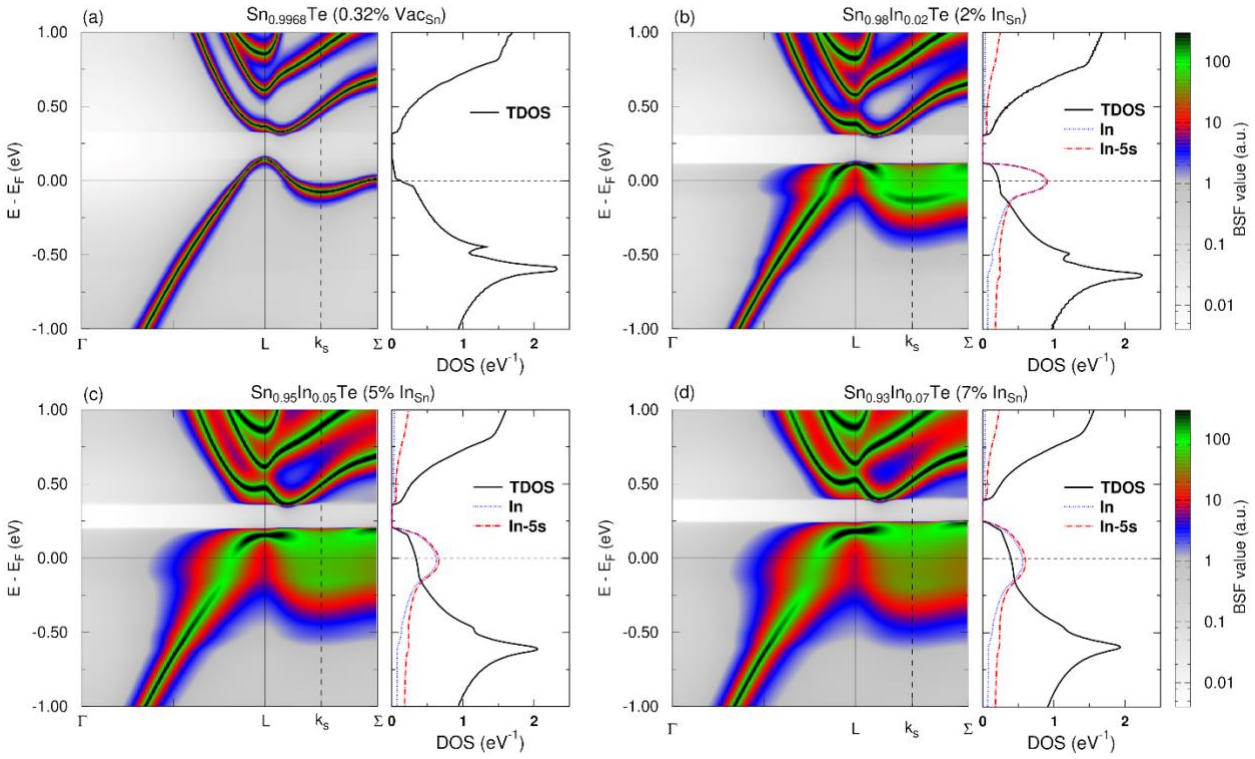
(a)
Sn0.9968Te (0.32% VacSn)
(b)
Sn0.98In0.02Te (2% InSn)
(c)
Sn0.95In0.05Te (5% InSn)
(d)
Sn0.93In0.07Te (7% InSn)
E - EF (eV)
1.00
0.50
0.00
-0.50
-1.00
Γ
L
ks
Σ
TDOS
In
In-5s
0
1
2
DOS (eV-1)
100
10
1
0.1
0.01
BSF value (a.u.)

Figure 1

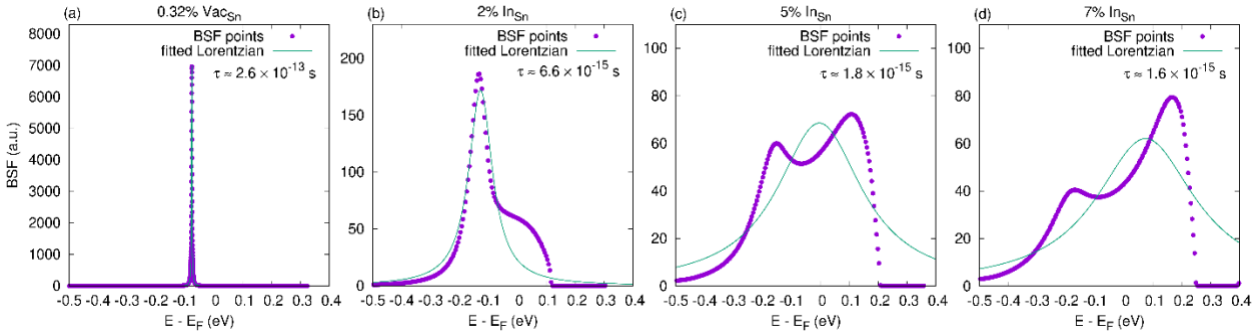
(a)
0.32% Vac$_{Sn}$
BSF points
fitted Lorentzian
$\tau \approx 2.6 \times 10^{-13}$ s
BSF (a.u.)
E - E$_F$ (eV)
(b)
2% In$_{Sn}$
BSF points
fitted Lorentzian
$\tau \approx 6.6 \times 10^{-15}$ s
E - E$_F$ (eV)
(c)
5% In$_{Sn}$
BSF points
fitted Lorentzian
$\tau \approx 1.8 \times 10^{-15}$ s
E - E$_F$ (eV)
(d)
7% In$_{Sn}$
BSF points
fitted Lorentzian
$\tau \approx 1.6 \times 10^{-15}$ s
E - E$_F$ (eV)

Figure 2

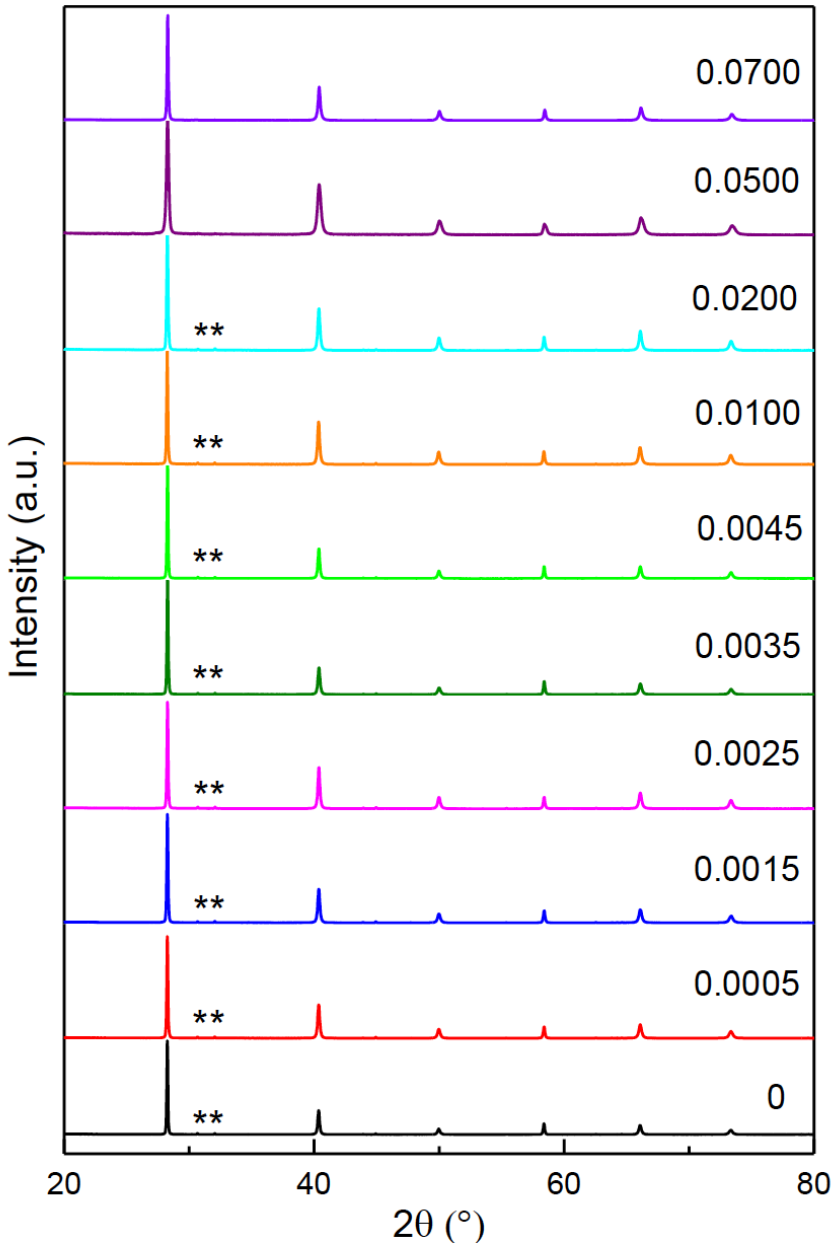
0.0700
0.0500
0.0200
0.0100
0.0045
0.0035
0.0025
0.0015
0.0005
0
**
Intensity (a.u.)
20
40
60
80
2θ (°)

Figure 3

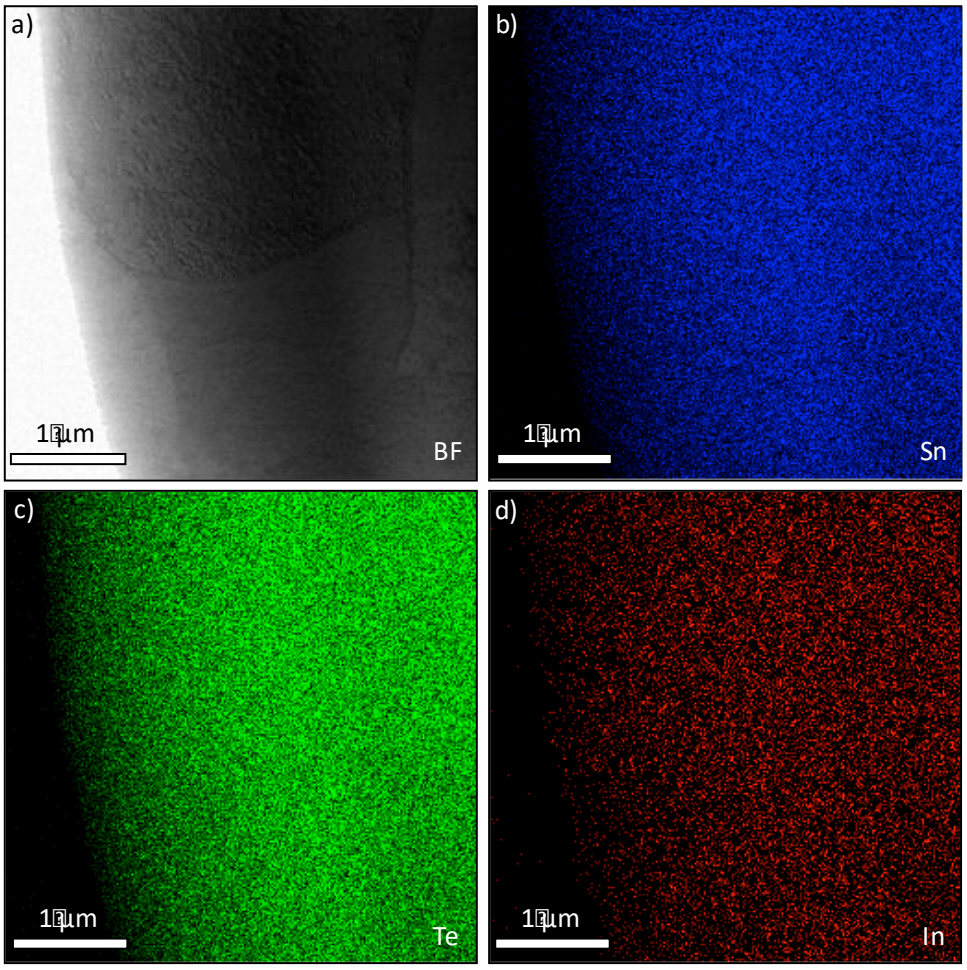

Figure 4

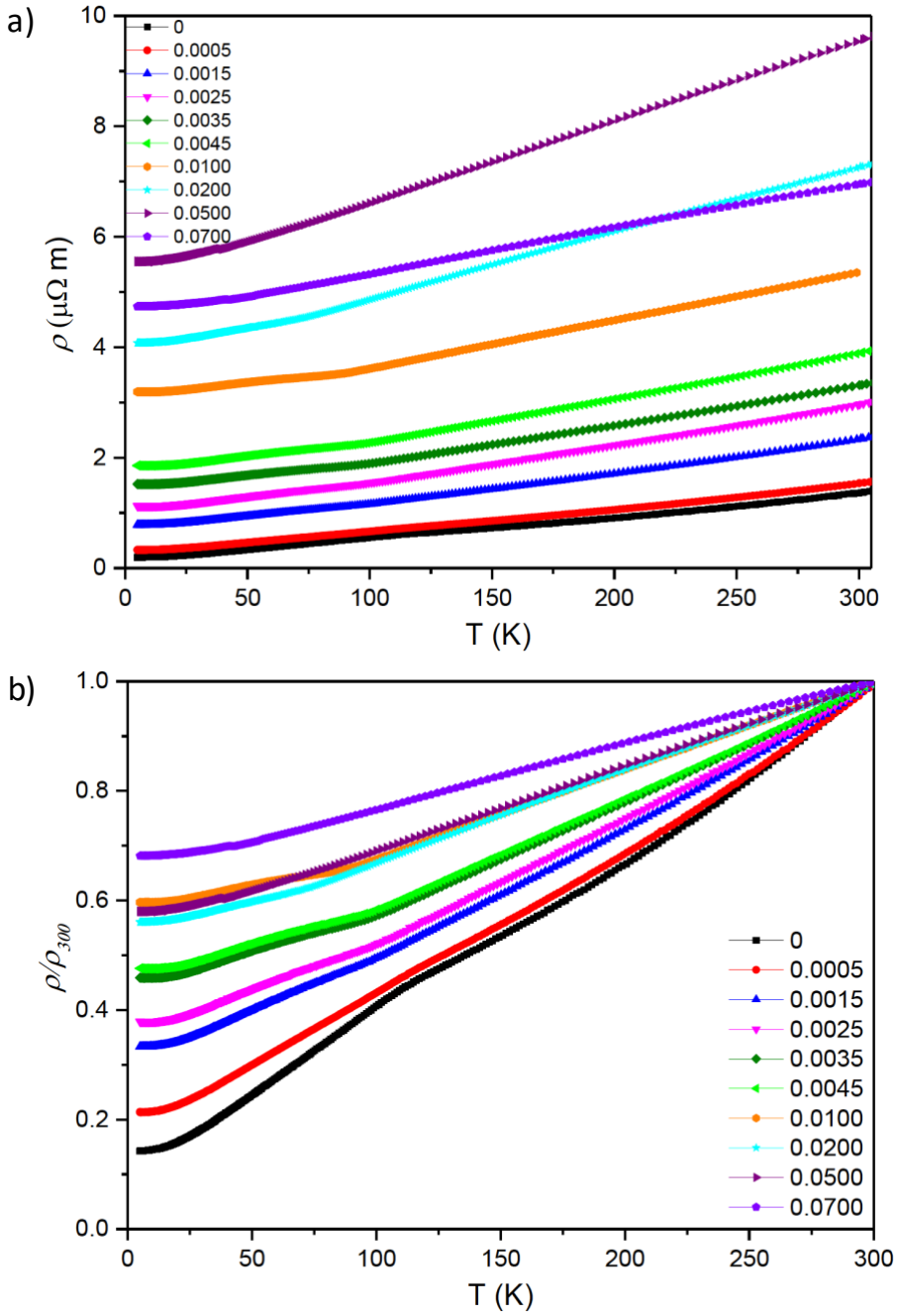
a)
ρ (μΩ m)
T (K)
0
0.0005
0.0015
0.0025
0.0035
0.0045
0.0100
0.0200
0.0500
0.0700
b)
ρ/ρ300
T (K)

Figure 5

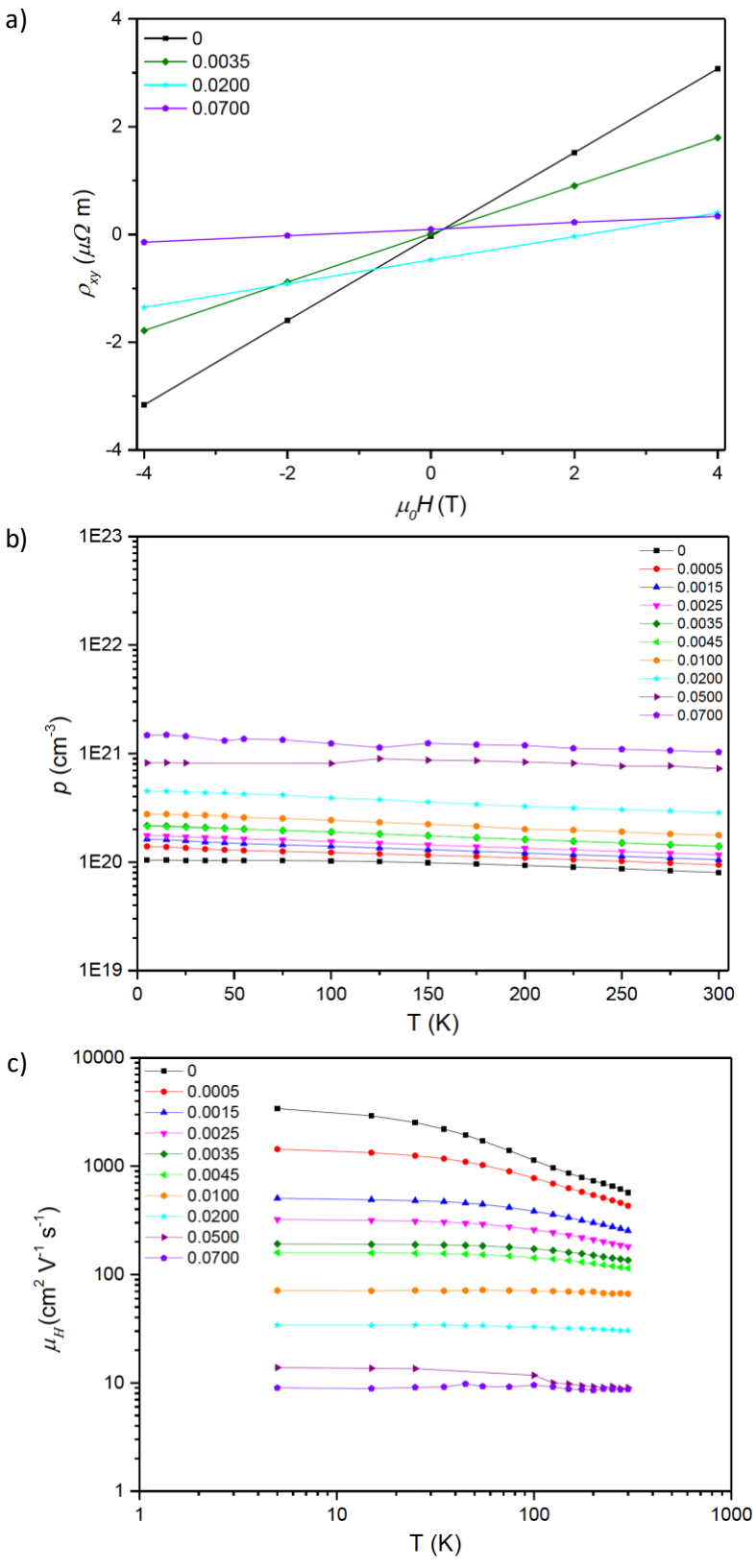
a)
0
0.0035
0.0200
0.0700
ρ_{xy} ($\mu\Omega$ m)
$\mu_0 H$ (T)
b)
0
0.0005
0.0015
0.0025
0.0035
0.0045
0.0100
0.0200
0.0500
0.0700
p (cm^{-3})
T (K)
c)
μ_H(cm^2 V^{-1} s^{-1})
T (K)

Figure 6

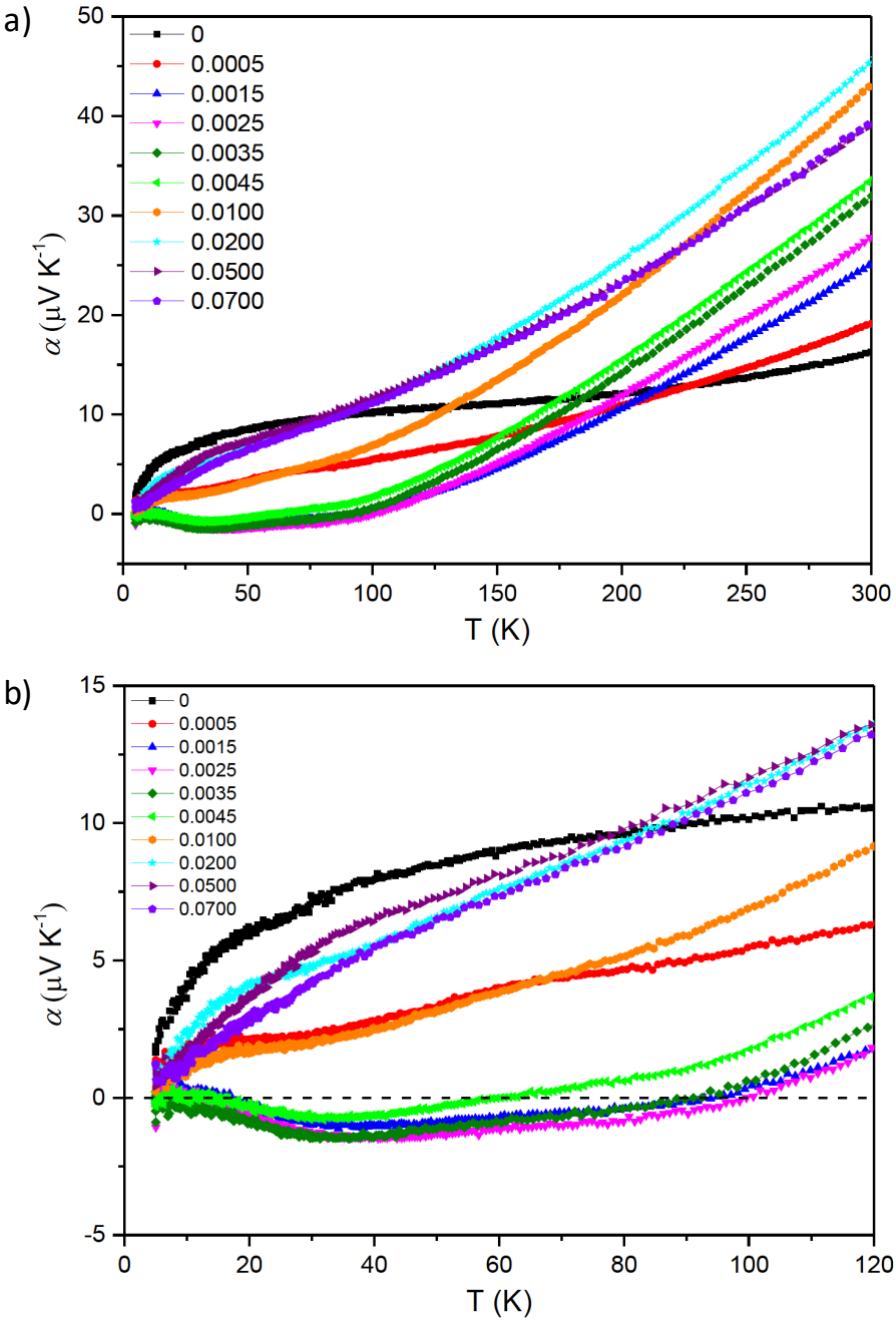
a)
0
0.0005
0.0015
0.0025
0.0035
0.0045
0.0100
0.0200
0.0500
0.0700
α (μV K-1)
T (K)
b)
0
0.0005
0.0015
0.0025
0.0035
0.0045
0.0100
0.0200
0.0500
0.0700
α (μV K-1)
T (K)

Figure 7

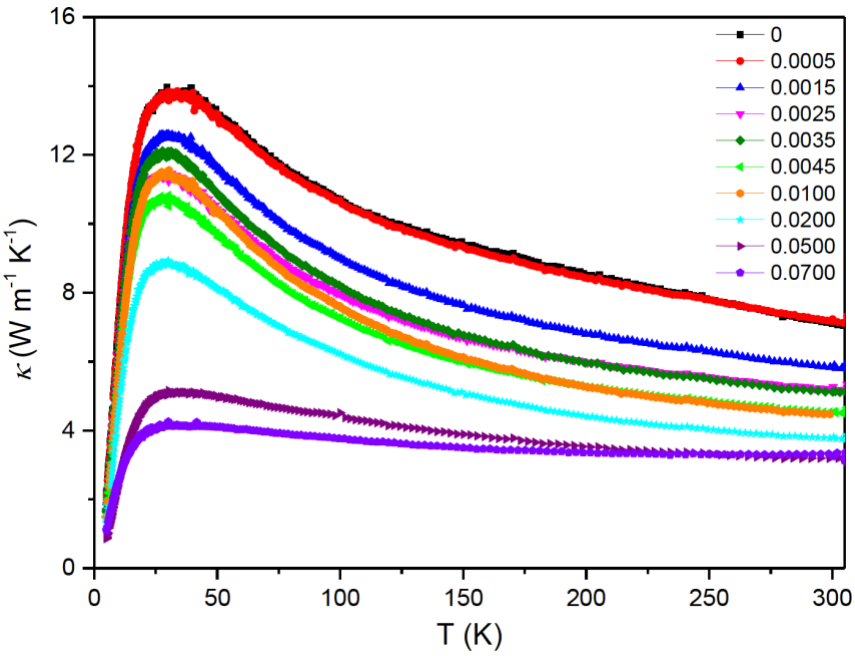
16
12
8
4
0
0
50
100
150
200
250
300
T (K)
κ (W m-1 K-1)
0
0.0005
0.0015
0.0025
0.0035
0.0045
0.0100
0.0200
0.0500
0.0700

Figure 8

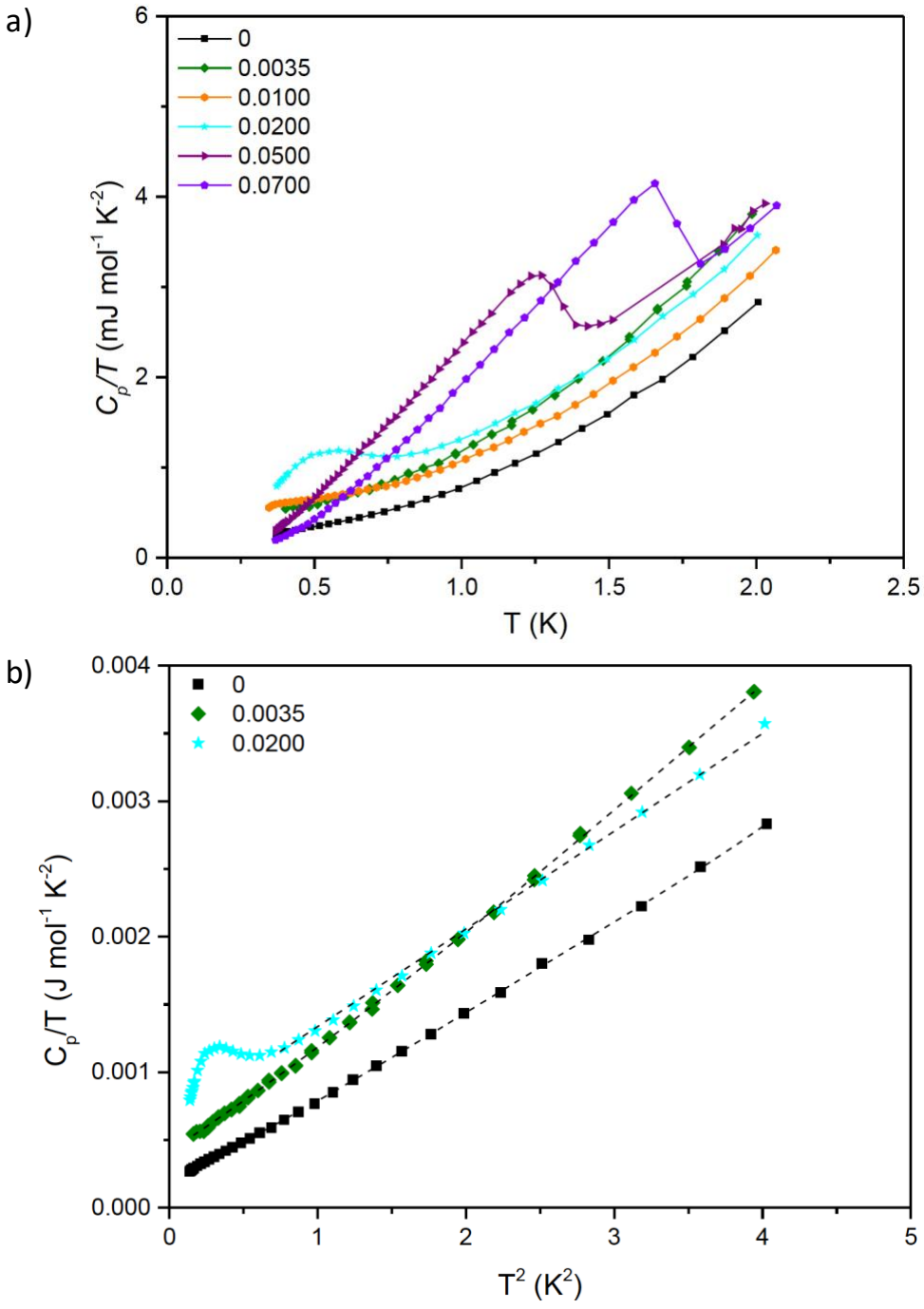
a)
0
0.0035
0.0100
0.0200
0.0500
0.0700
C_p/T (mJ mol^{-1} K^{-2})
T (K)
b)
0
0.0035
0.0200
C_p/T (J mol^{-1} K^{-2})
T^2 (K^2)

Figure 9

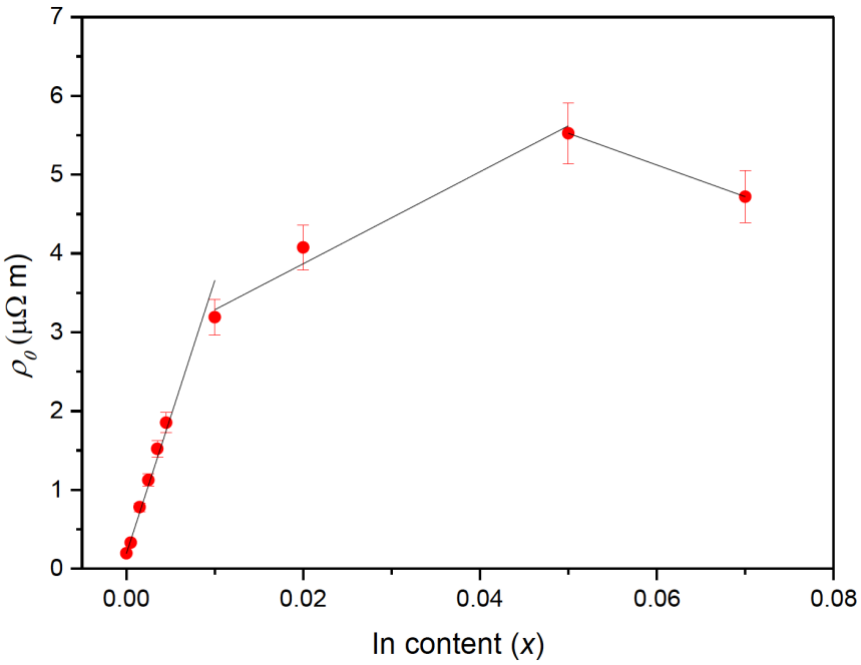

Figure 10

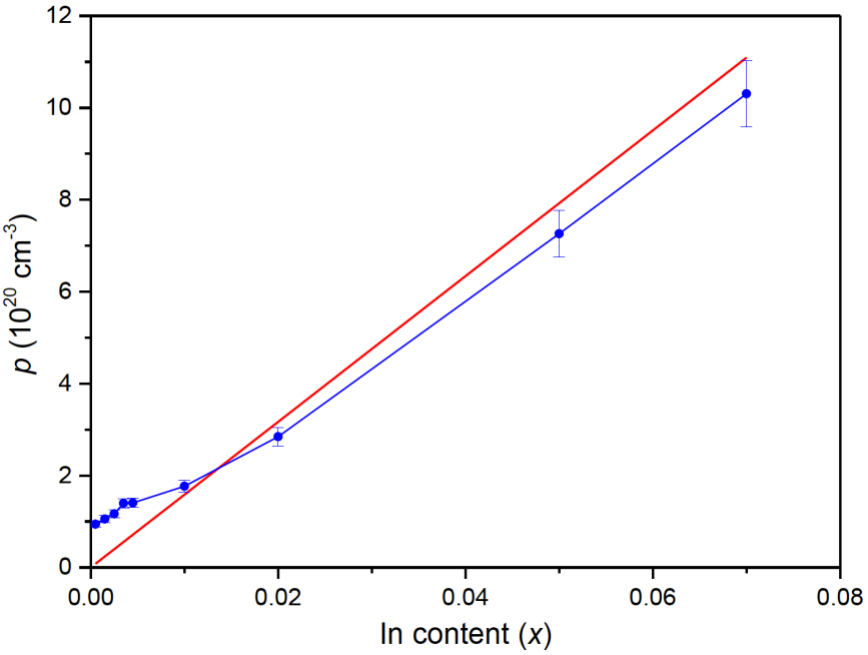

Figure 11

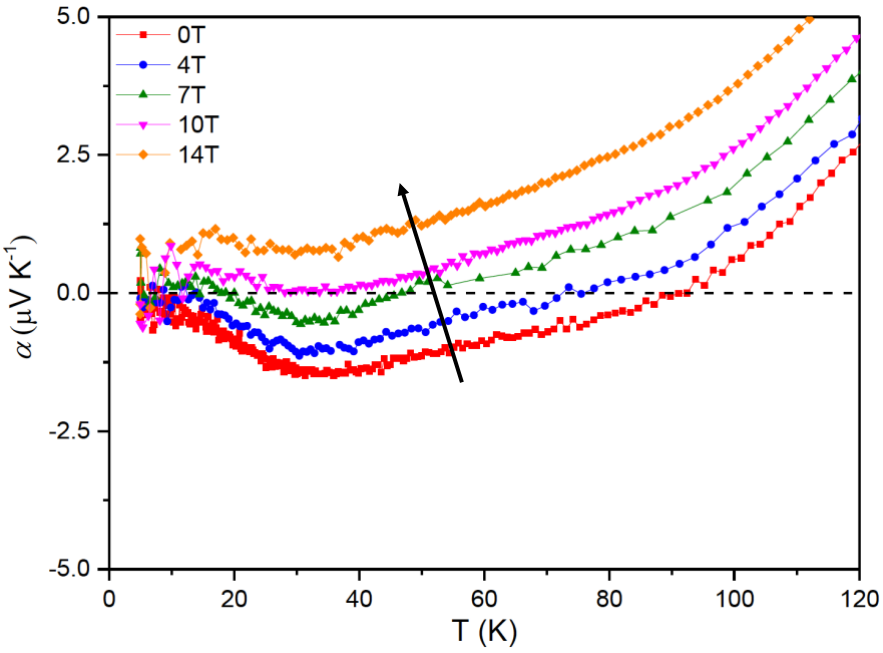

Figure 12

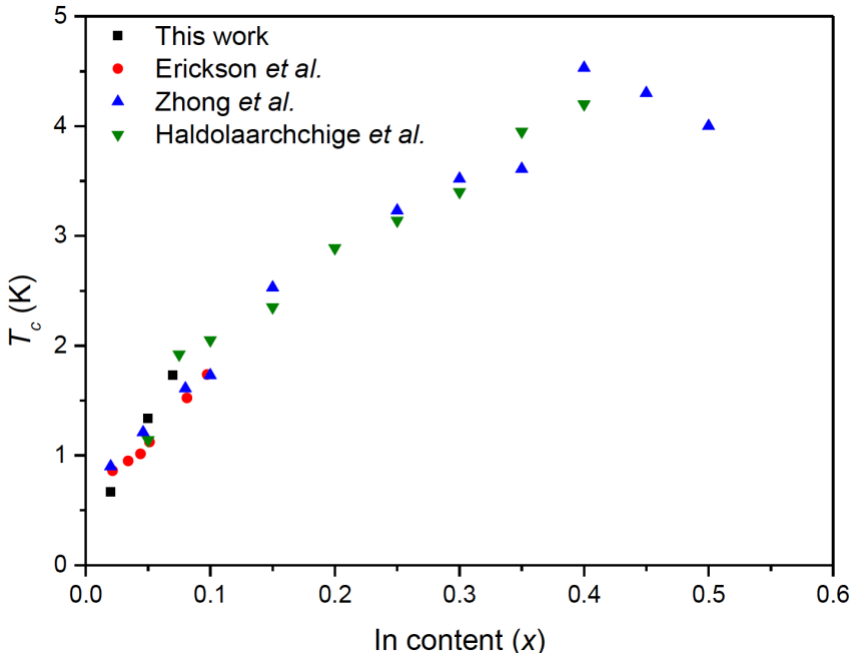
This work
Erickson et al.
Zhong et al.
Haldolaarchchige et al.
T_c (K)
In content (x)
0
1
2
3
4
5
0.0
0.1
0.2
0.3
0.4
0.5
0.6

Figure 13